Co-funded by the Erasmus+ Programme of the European Union

Innovative Pedagogical Tools

Sites visits

Learning by doing

Summary report **Intellectual Output 6**

Table of Contents

1 Introduction 6
2 Operating geothermal facilities visits 7
2.1 Low Enthalpy geothermal systems 7
2.1.1 Greenhouses 8
2.1.2 Eco district 9
2.1.3 High School heat energy supply 10
2.2 High Enthalpy geothermal systems 11
2.2.1 Geothermal exploitation sites within the Upper Rhine Graben 11
2.2.2 Geothermal exploitation sites within the Pannonian basin 16
2.2.3 Geothermal exploitation sites within an oceanic rift area 18
3 Geological excursions and data analysis on geothermal reservoir analogues 21
3.1 Sedimentary basins 21
3.1.1 The Pannonian basin 21
3.1.2 The Aquitaine Basin 29
3.2 Rift type basins with fractured basement rocks 37
3.2.1 The Gabe Gottes Mine in the Vosges moutains (Alsace, France) 40
3.2.2 The Teufelsgrund and Schauinsland mines (Black Forest, Germany) 44
3.3 Volcanic areas 52
3.3.2 Þjórsárdalur (Gjáin and Háifoss) 58
3.3.3 Landmannalaugar and the Torfajökull Volcano 59
3.4 Orogen foreland domain 62
4 Petrophysical investigations in the laboratory 65
4.1 Permeability and porosimetry 65
4.2 Thermophysics laboratory 66
4.3 Rock mechanics laboratory 66
4.4 Thermotriax facility 66
5 Turbine engineering 69
5.1 Turbine types 69
5.2 Steam turbines 69
5.3 Turbines for organic fluids 71
5.4 Water turbines 74
6 Environmental Impact Site-Visits 77
6.1 Þjórsárdalur 77

6.2 Burfellstöð & Gjáin 79
7 Summary 81

Table of Figures:

Figure 1: Lindal diagram of geothermal heat direct uses according to temperature ranges. (Source: Gehringer and Loksha, Geothermal Handbook: Planning and Financing Power Generation, ESMAP 2012) 7
Figure 2: Position of potential heat end-users identified near Vermilion sites in France 8
Figure 3: Heat network connecting Vermilion Parentis depot and Tom d'Aqui greenhouses 9
Figure 4: Geographic location of the eco-district project 10
Figure 5: Location of the petroleum site related to end-user and position of the buried pipe 11
Figure 6: Equilibrium temperature profile obtained from log run GPK2 several months after drilling operation finished. Main geological units are presented versus depth. (Genter, 2010) 12
Figure 7: ISP students at the Soultz sous Forêts geothermal power plan (France) 13
Figure 8: Temperature profile at Rittershoffen site (France) 14
Figure 9: ISP students at the Rittershoffen geothermal power plan (France) 15
Figure 10: ISP students at the Insheim geothermal power plan (Germany) 16
Figure 11: Well temperature profiles at the Ciglena geothermal power plan (Croatia) 17
Figure 12: ISP students at the Ciglena geothermal power plan (Croatia) 18
Figure 13: Map of Hengill area showing surface contours, eruptive fissures and mapped fractures. Well tracks are shown in red. From Gunnarsson et al, 2021. 19
Figure 14 ORC view at Hellisheidi powerplant 20
Figure 15: Map of principal tectonic and geographic units of the Alps, Carpathians, Dinarides and the Pannonian Basin with its subbasins and depocentres (Cvetković, 2019) 22
Figure 16: Map of Moho discontinuity depths in SE Europe (Grad et al. 2009) 23
Figure 17: Terrestrial heat flow density in Croatia (Hurtig et al., 1992) 24
Figure 18: Croatian part of the Pannonian basin system 25
Figure 19: Tectonic map of the Velika Ciglena geothermal reservoir 26
Figure 20: Longitudinal cross – section across the VC-1 and VC-1a wells 26
Figure 21: Schematic geological cross-section, redrawn according to Zelić et al. (1995) 27
Figure 22: Project of seismic and borehole data in the MOVE software by Borović et al (2021) 28
Figure 23: Localisation of Plage de Gurp 30
Figure 24: Geological map of plage de Gurp area. See figure for legend. BRGM geological map St Vivien de Médoc / Soulac sur Mer XIV - 33 32
Figure 25: Glacial period deposits interpretation. Geological cross section, see map trace in figure 26 33
Figure 26: Panoramic view of the investigated outcrop 34
Figure 27: Close up on the stratigraphic succession consisting in two impermeable organic rich layers from the Gurp formation. 35
Figure 28: Panoramic view of the dune system overlying the investigated outcrop 36

Figure 29: a) Simplified geological map of the Upper Rhine Graben and surrounding low mountain ranges, as well as basins including structural settings of selected high temperature areas of b) Soultz sous Forêts and Rittershoffen and c) Landau and Insheim 38
Figure 30: Simplified geological cross sections and isotherms obtained from geostatistical modeling across Soultz and Rittershoffen geothermal fields (AB in Figure) and across Landau and Insheim geothermal fields (A'B') in Figure 31 39
Figure 31: ISP students at the Kaiserstuhl summit, at the Rhine Graben center. Panorama analysis. 40
Figure 32: Tectonic phases of the Vosges mountains since the Carboniferous to the end of the Miocene (Hafeznia et al. 2015) 41
Figure 33: Geological map of the Gabe Gottes mine with fault analysis data 42
Figure 34: Interaction between a sheared zone and euhedral – geodic veins 43
Figure 35: Geological map of the Black Forest. In red, the location of the detailed geological map of the Schauinsland area, translated after Wittenbrink (1999) 45
Figure 36: a) ore mineral vein in Schauinsland showing evidence of brine circulation pulses, b) N-S cross-section of Schauinsland showing the Schumachersche Ruschel cross_cutting the massif, modified after Wittenbrink 1999 46
Figure 37: Geological map of the gallery, the studied area corresponds to the red rectangle where the beginning of the gallery is on the left, modified and translated after (Wittenbrink, 2002). 47
Figure 38: Photogrammetric model of the portion of the gallery showing the fault gouge 48
Figure 39: Scheme of the extinction of the mineral vein when encountering the highly strained shear zone (Werner, 2002) 49
Figure 40: ISP students and accompanying staff at the Teufelsgrund mine entrance 50
Figure 41: Geological overview presentation to ISP students within the Schauinsland mine 50
Figure 42. Main Volcanic zones in Iceland. Reykjanes Volcanic Belt (RVB), the West Volcanic Zone (WVZ), the Mid-Iceland Belt (MIB), the East Volcanic Zone (EVZ) and the North Volcanic Zone (NVZ). Two transform zones are connecting these volcano-tectonic zones: the South Iceland Seismic Zone (SISZ) in the south of Iceland and the Tjörnes transform Fault Zone (TFZ) in the north. Outside of the main island are the Reykjanes Ridge (RR), as part of the Mid-Atlantic Ridge to the southwest and the Kolbeinsey Ridge (KR) to the north. 53
Figure 43. ISP field excursion in Iceland 54
Figure 44. The main tectonic structures of the Reykjanes Peninsula. The volcanic systems are in pink, the seismic zone (the plate boundary) is in red and the geothermal systems are shown in yellow. The offshore trace of the plate boundary is in black. Modified from Hersir et al (2020). 55
Figure 45. An overview of Krysuvik. Fumaroles, fractures and faults are according to a recent geological mapping by Saemundsson et al. (2016).Wells deeper than 300mandwell KR-01 andwell KR-03 are denoted by red filled triangles, fumaroles by green/yellowstars and fractures and faults bymagenta lines. Blue colour denotes the ocean and lakes. Modified from Hersir et al (2020). 56
Figure 46. Activity at Seltún, showing acidic mud pools and hydrothermally altered rock, with a carapace of less intensely-altered subglacial basaltic deposits. Photo J. Newson. 57
Figure 47. ISP students at Fagradalshraun. This is only part of the ISP Iceland class; the others walked further to investigate the lava textures and how they might be analogues for subsurface permeability in a volcanic-hosted reservoir. Photo J. Newson. 58
Figure 48. Geological map of the Gjáin-Háifoss area from https://orkustofnun.is/vefsjarmyndir/1028.jpg . The yellow arrows point to the locations of Háifoss and Gjáin. Symbols for the lithologies are:

thi=Búrfellshraun; stþ=Stangarfjall tholeiite; sao=Sandafell olivine tholeiite; smd=Sámsstaðamúli porphyritic basalt; rep=Reykholt tholeiite; rem=Reykholt hyaloclastite. 59
Figure 49. The Torfajökull Volcanic area, showing Landmannalaugar on the northern edge of the caldera (adapted from Björke et al, 2015). 60
Figure 50. Geologic map of the northern margin of the Torfajökull Volcano, showing the Laugahraun (underlined in yellow), and the Landmannalaugar area to the northeast of the lava flow (from https://orkustofnun.is/vefsjarmyndir/873.jpg). 61
Figure 51. Students on the surface of the Laugarhraun flow, near steam activity (background middle left). Photo J. Newson. 61
Figure 52. geological map from Ford et al. 2002, representing the main domains of southern sub alpine foreland basins. 63
Figure 53. Regional cross-section in the southern Alps, between Digne and Colmars (Menut et al., 2022). 64
Figure 54. Hydrothermikum lab visit and experimentation from students to characterize multi parameters petrophysical behavior of rock samples 67
Figure 55. ISP Students performing experiments with mentoring in the Thermo-triax facility necessary for optimal permeabilities for geothermal reservoir rocks samples. 68
Figure 56. Flow diagram of a flash steam geothermal power plant (El Haj Assad et al., 2017) 69
Figure 57. Multistage steam turbine (Chisley and Prescott, 2013) 70
Figure 58. ISP students at the EL-TO Zagreb thermal power plan (Croatia) 71
Figure 59. Flow diagram of geothermal power plant with binary cycle (Franco et al., 2017) 72
Figure 60. Temperature-entropy diagrams of organic fluids (Lee and Kim, 2015) 72
Figure 61. Radial outflow turbine used in geothermal power plant with binary cycle (Franco et al., 2017) 73
Figure 62. Housing of a turbine used in power plant Velika 1 74
Figure 63. Students in front of the Kaplan turbine in hydro power plant Varaždin in Croatia. 75
Figure 64. Pelton hydraulic turbine and synchronous generator at University of Zagreb 76
Figure 65: Outline of Protected Area in Þjórsárdalur with proximity of Þjórsá power stations 78
Figure 66: Þjórsárver Protected Areas 79
Figure 67: Geo3en ISP students at Gjáin 80

1 Introduction

The Geo3EN project aims at elaborating a global teaching program in the domain of geothermal engineering. The program is guided by the idea that a direct application of the theoretical knowledge received in either the laboratory, the field, or on production sites is the most efficient way of dealing with real case scenario challenges.

Taking into account the extraordinary variety of competences required to the geothermal engineer like dealing with a broad spectrum of geothermal reservoir conditions and surface infrastructures technologies to name just a few, putting directly into practice the acquired fundamental knowledge is to be preferred.

In order to achieve this goal, students are given the opportunity to

1) visit running geothermal facilities and discuss with sites owners operating at various exploitable enthalpy conditions,
2) investigate geothermal reservoir analogues on sedimentary basins, volcanic areas and orogen foreland domains,
3) test reservoir rocks petrophysical properties and power plans components efficiency in the laboratory.

In the following, site owners willing to give access to operating geothermal facilities are given with a condensed description of their installation characteristics. A similar list presenting pedagogically relevant reservoir analogues and laboratory testing facilities is presented.

Some of these sites (power plans, reservoir analogues and laboratories) have been extensively used in the framework of the Intensive Study Program during the period April – June 2022.

2 Operating geothermal facilities visits

The present level of engineering knowledge and technology permits geothermal energy extraction, transformation and use over a wide enthalpy range. For this reason, geothermal installations are found in low temperature conditions at sub surface down to hot and superhot conditions in deeply buried reservoirs.

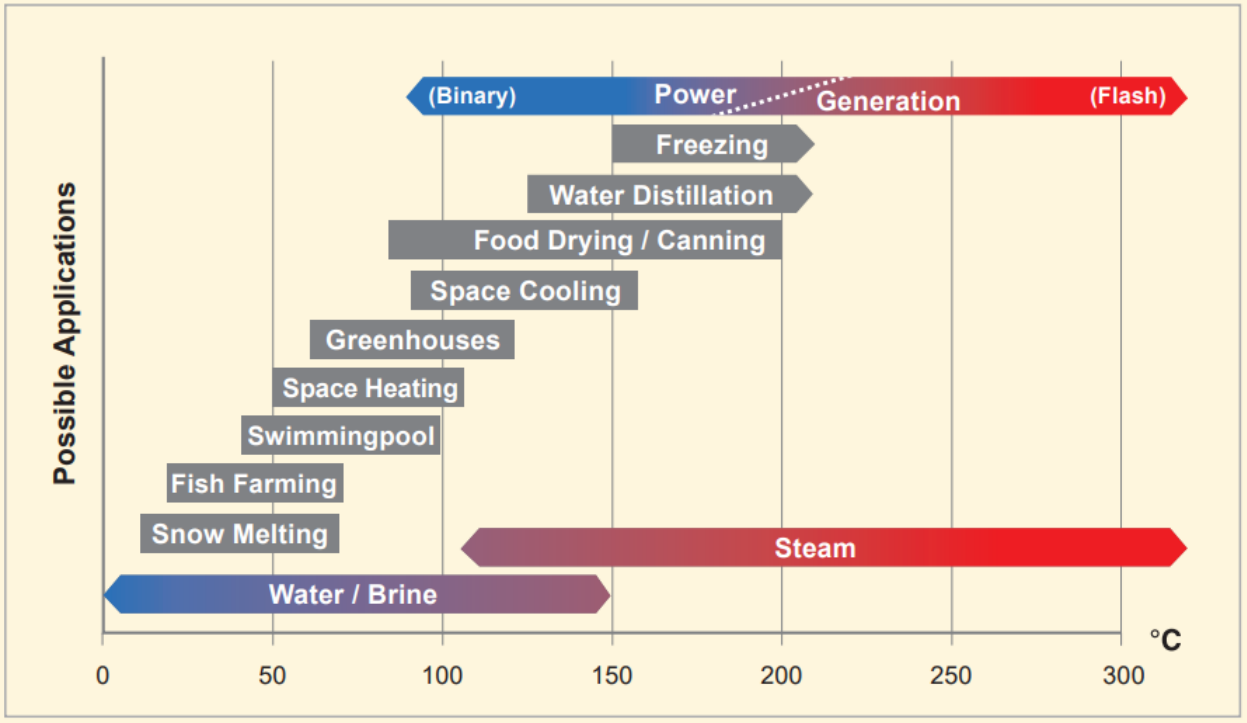

Figure 1: Lindal diagram of geothermal heat direct uses according to temperature ranges. (Source: Gehringer and Loksha, Geothermal Handbook: Planning and Financing Power Generation, ESMAP 2012)

The Geo3EN program offers the possibility to students to visit several types of operating installations at both low and high enthalpy geothermal systems (Figure 1).

2.1 Low Enthalpy geothermal systems

Students are given the opportunity to visit low enthalpy exploitation sites within the Paris and Aquitanian basins in France. Geothermal brines are being co-produced from mature oil fields exploited by the Vermilion company.

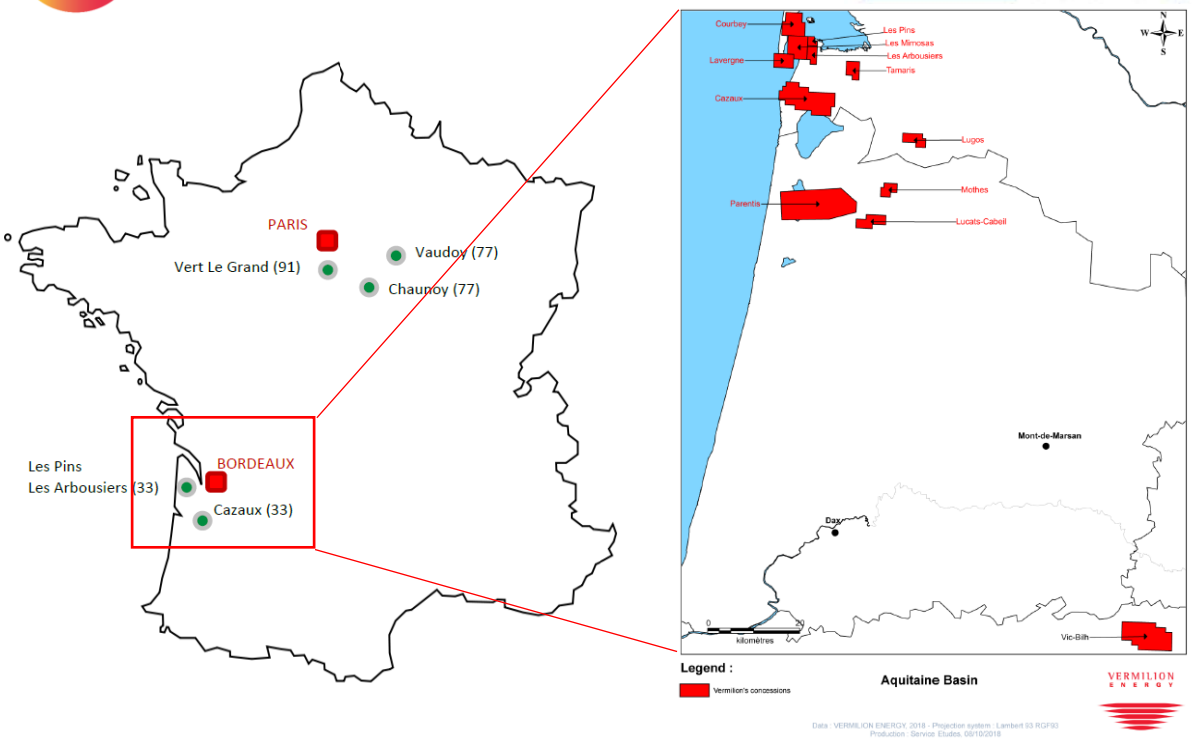

Figure 2: Position of potential heat end-users identified near Vermilion sites in France

Within the Aquitanian basin, geothermal brines at temperatures between 50°C and 70°C are used for either space heating and greenhouses (Figure 2).

2.1.1 Greenhouses

Vermilion's resource is already used by Tom d'Aqui, a tomato greenhouse grower, to heat up 15ha of green house at Parentis oil facilities since 2008 (Figure 3).

At the beginning of their activity, the 8 MW available on the Parentis site were sufficient to cover the heat needs of the first 6.5-hectare greenhouse built. Then, as Tom d'Aqui have extended their activity, now representing a total surface of 10 hectares, Vermilion's geothermal heat needs to be assisted by another source of energy: gas is the solution chosen by Tom d'Aqui.

Tom d'Aqui declared that they cannot be fully dependent on geothermal energy only. Indeed, if Vermilion's oil production has to be stopped for any reason or if the temperature fluctuates, they need a backup solution.

Their energy mix is as followed:

- Greenhouses' heat needs are mainly supplied by Vermilion's geothermal heat
- Gas produced by co-generation activity constitutes their backup solution
- A wood-fired boiler is also on site but is currently not in operation: this installation is the gas' backup solution.

The greenhouse needs about 60 GWh / year, covered at 80% by geothermal resource.

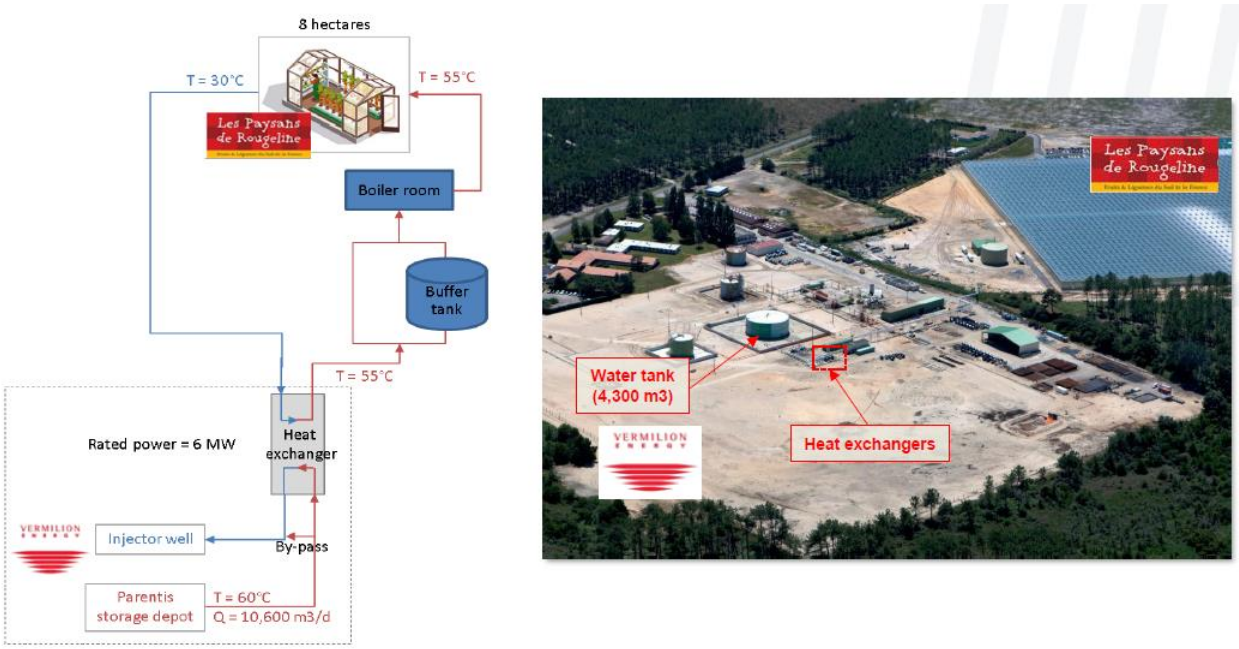

Figure 3: Heat network connecting Vermilion Parentis depot and Tom d'Aqui greenhouses

2.1.2 Eco district

Among the different concessions owned by Vermilion in France, the one located in La Teste produces hot water which is used since July 2017 to supply heat for the Eco-district Les Portes du Pyla, in La Teste-de-Buch (Figure 4). That energy is exploited through a win-win partnership with ENGIE Cofely, which is a French leader company in heating networks and renewable energy services for districts and municipalities.

Water is separated from the oil and gas is characterized by a temperature of 70°C and a volumetric flow of 850 m3/d. Considering a temperature of 50°C at the injector well, the theoretical thermal power available at this site is estimated at 800 to 900 kW.
To extract the thermal heat from the geothermal resource, a counter-flow plate heat exchanger was installed. This 79-titanium-plate heat exchanger was designed for a thermal power equal to 800 kW.

The eco-district Les Portes du Pyla, located in La Teste-de-Buch, covers over 11ha and represents 500 equivalent residential units. 80% of its energy mix is covered by geothermal heat supplied by Vermilion. The 20% left are from gas-based origins and supplied by ENGIE Cofely.
Thanks to this free heat supplied by Vermilion, ENGIE Cofely is able to offer heat to end consumers at a competitive cost: 50% savings have been achieved and geothermal resource covers almost 80% of the needs.

Figure 4: Geographic location of the eco-district project

2.1.3 High School heat energy supply

The Condorcet high school is located in Arcachon, SW of France (Figure 5). It welcomes 700 pupils, and has yearly heating needs of 850 MWh, provided by gas boiler emitting 230 tons of CO2 per year. This project is expected to cover more than 90% of heating needs and save 190 tons of CO2 per year.

The end -user is located 250 m away from the oil facilities. A heat exchanger has been added right before the injection wells where heat is transferred to a buried secondary pipe loop.

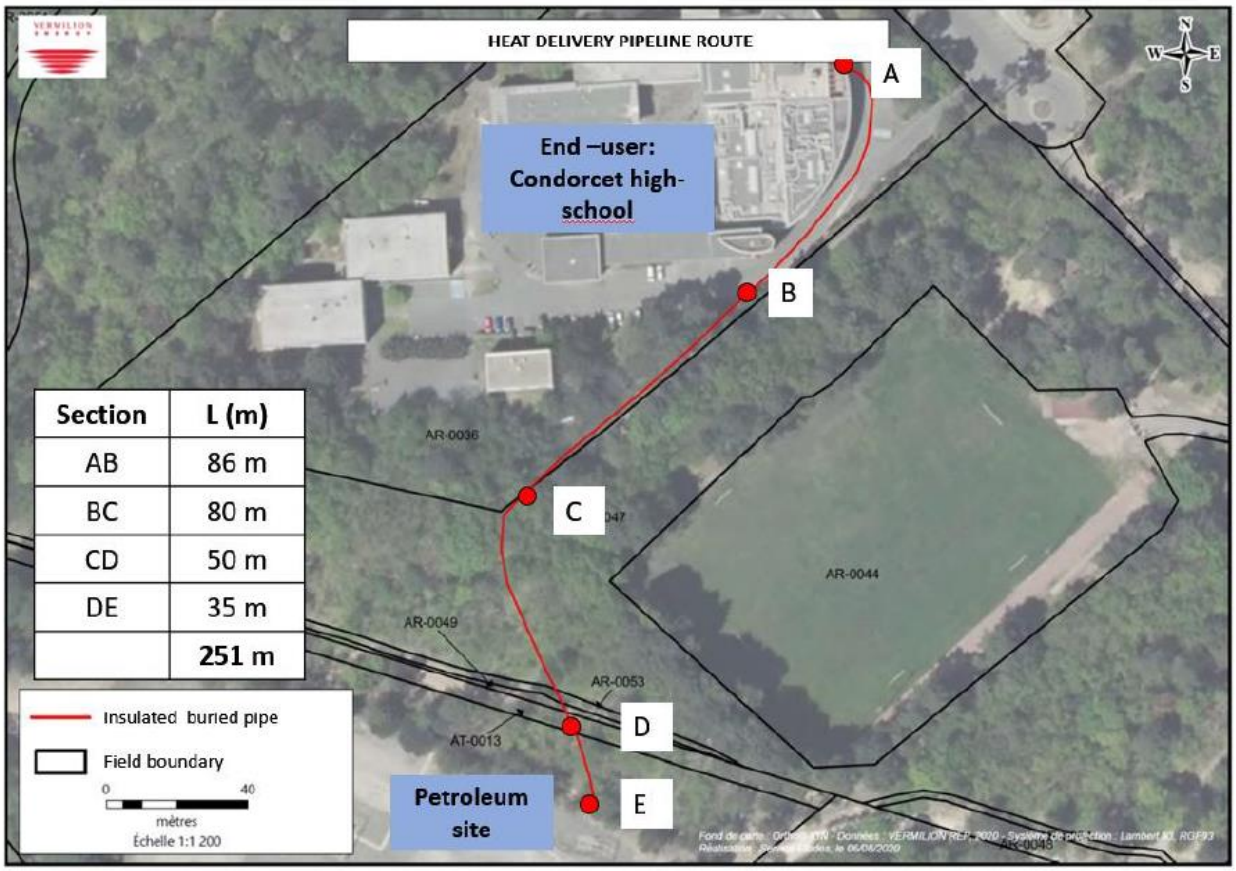

Figure 5: Location of the petroleum site related to end-user and position of the buried pipe

2.2 High Enthalpy geothermal systems

Students are given the opportunity to visit high enthalpy exploitation sites within the French, German, Croatian and Icelandic territories. Geothermal brines are being extracted either from fractured basement rocks from a continental rift system (Upper Rhine Graben), from sedimentary basin (Pannonian basin) or from an oceanic rift volcanic setting (Iceland).

2.2.1 Geothermal exploitation sites within the Upper Rhine Graben

2.2.1.1 The Soultz sous Forêts power plan (France)

The Soultz-sous-Forêts EGS (Enhanced Geothermal System) power plant is located in Northern Alsace in the Upper Rhine Graben (URG).

It consists of several deep wells drilled in a Palaeozoic granite reservoir at a depth of 5km (Genter, 2010) (Figure 6).

The owner of the Soultz plant is the “GEIE Exploitation Minière de la Chaleur”, while the geothermal plant operation and maintenance is performed by ES-Géothermie.

Currently, the geothermal site exploits around 30 L/s of geothermal water with a very high salinity of 100 g/L. The brine is produced at 150°C from the production well GPK-2 and conveyed after filtration to three heat exchangers supplying heat to a 1.7 MW ORC unit. This electricity production unit is the only heat user of this geothermal plant, and uses the ambient air as a heat sink, through an Air-Cooled Condenser. The ambient air temperature variations throughout the day and the year impact the geothermal brine reinjection temperature, ranging from 60°C to 80°C.

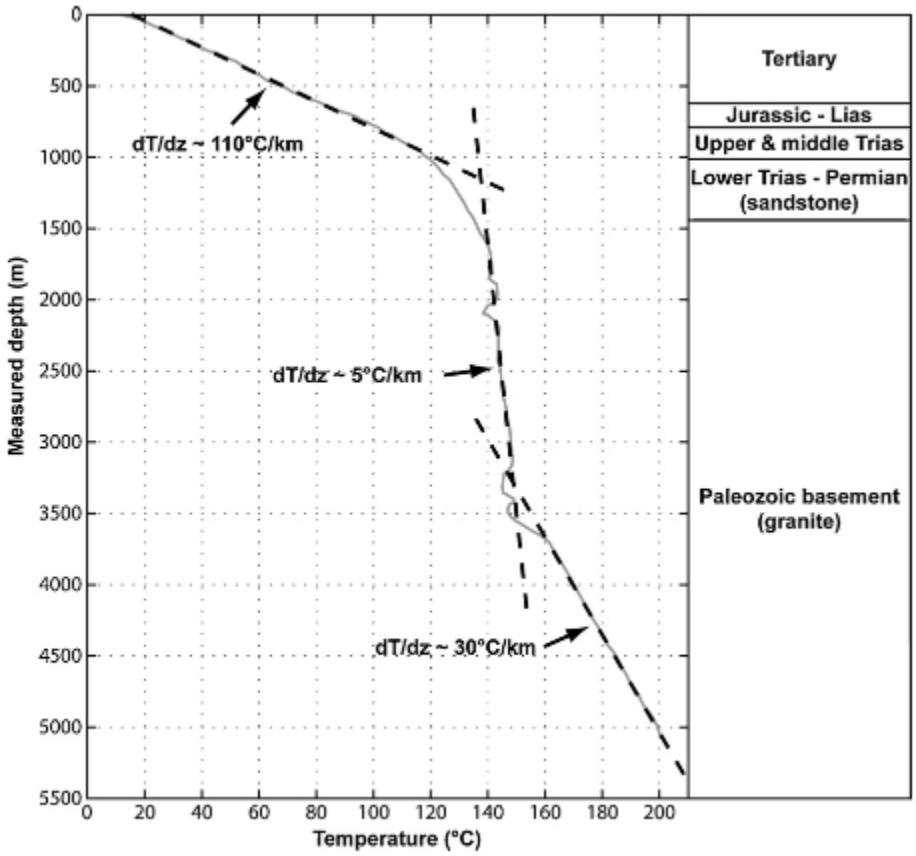

Figure 6: Equilibrium temperature profile obtained from log run GPK2 several months after drilling operation finished. Main geological units are presented versus depth. (Genter, 2010)

The geothermal brine is reinjected into two different wells, GPK-3 and GPK-4. The geothermal plant is fully operational since mid-2016, when a new ORC unit was erected and the geothermal loop refurbished.

Figure 7: ISP students at the Soultz sous Forêts geothermal power plan (France)

This power plant was visited on May 13th 2022 by ISP students and accompanying staff members under guidance of Dr. Albert Genter (Figure 7).

2.2.1.2 The Rittershoffen power plan (France)

The power plan delivers geothermal heat to the Roquette Frères corn starch company in the city of Beinheim 15 km away from the Rittershoffen site.

The plan was built within the ECOGI project (Exploitation de la Chaleur d'Origine Géothermale pour l'Industrie) with a joint venture of 40% ES (Electricité de Strasbourg), 40% Roquette Frères and 20% Caisses des dépôts.

Two wells at 2500 m depth allow extraction of brines at a temperature of 170°C (Figure 8) and re injection at 70°C.

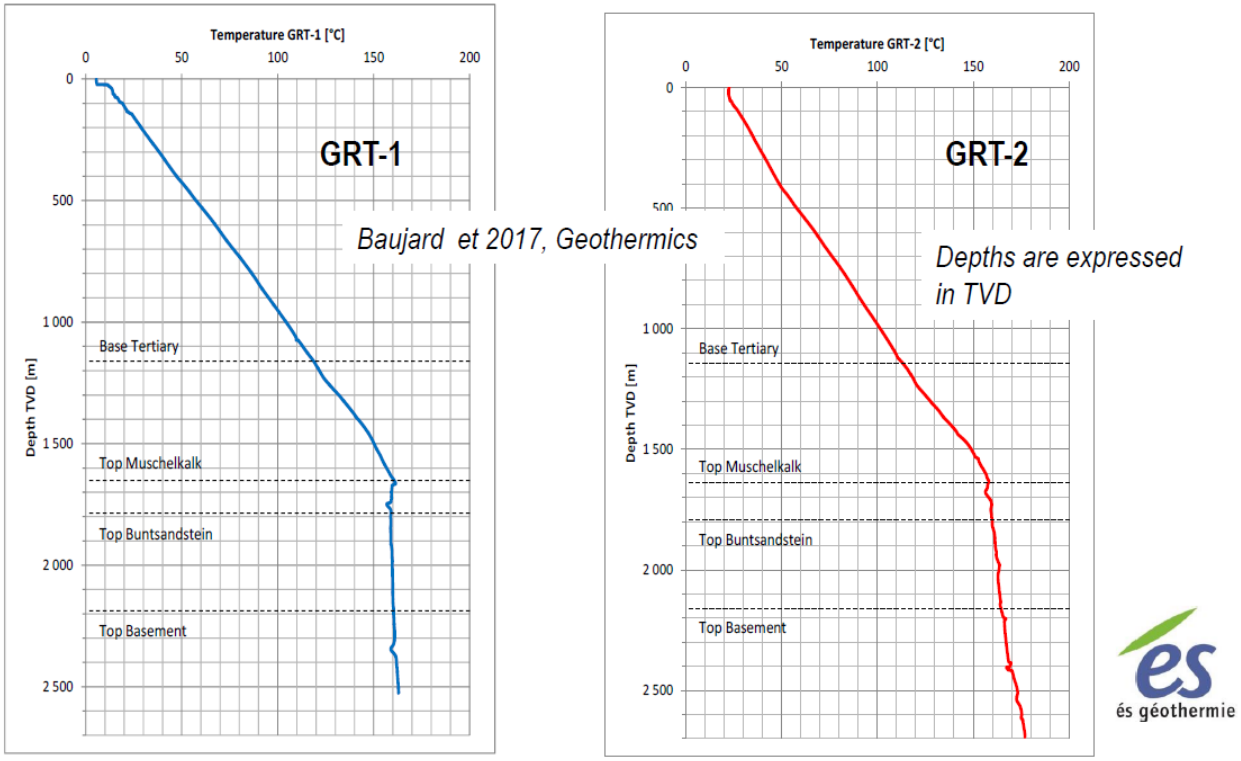

Figure 8: Temperature profile at Rittershoffen site (France)

The average flow rate is of 250 m^3 / hour with an installed capacity of 27 MW and an average user power of 22MW. The annual production is of 180 GWh with an availability higher than 8000 h / year.

This production covers 25% of the Roquette company heat needs and saves 41 000 t of CO_2 per year.

Figure 9: ISP students at the Rittershoffen geothermal power plan (France)

This power plant was visited on May 13th 2022 by ISP students and accompanying staff members under guidance of Dr. Albert Genter (Figure 9).

2.2.1.3 The Insheim power plan (Germany)

The Insheim site is located in the Upper Rhine Graben in Germany, about 30 km North of Soultz-sous-Forêts, France. Since 2012 the operator, Pfalzwerke geofuture GmbH generates 4.8 MW of electric power from a geothermal power plant using a single fault system in the crystalline rock for heat extraction covering the needs of approximately 8000 households. The brine flow rate reaches an average of 85 L/s.

In 2008 and 2009 two wells, one injector and one producer, were successfully drilled to a depth of about 3800 meters.

In autumn 2010 a lateral drain was drilled out of the injection well at approximately 2500 meters, aiming at better distributing the flow between two injection branches and thus minimizing the induced microseismic activity.

Figure 10: ISP students at the Insheim geothermal power plan (Germany)

This power plant was visited on May 13th 2022 by ISP students and accompanying staff members under guidance of Mrs. Kraeh (Figure 10).

2.2.2 Geothermal exploitation sites within the Pannonian basin

The Velika Ciglena project is located in the Northeast part of Croatia, where in the early 90's, during an Oil&Gas exploration, an unexpected high temperature water was found (about 170°C). The reservoir was discovered in 1990 by the VC-1 well within the scope of exploration for oil, conducted by INA-Naftaplin. Oil was not found, but a promising geothermal potential was established. A casing was lowered into the well at the depth of 2574 m. An unusually high temperature (172 °C) was registered for the region. Currently, four deep wells are located on the project area (Figure 11). The selected configuration is to use wells VC-1 and VC-1A as production wells while VC-2 and PTK-1 are injection wells.

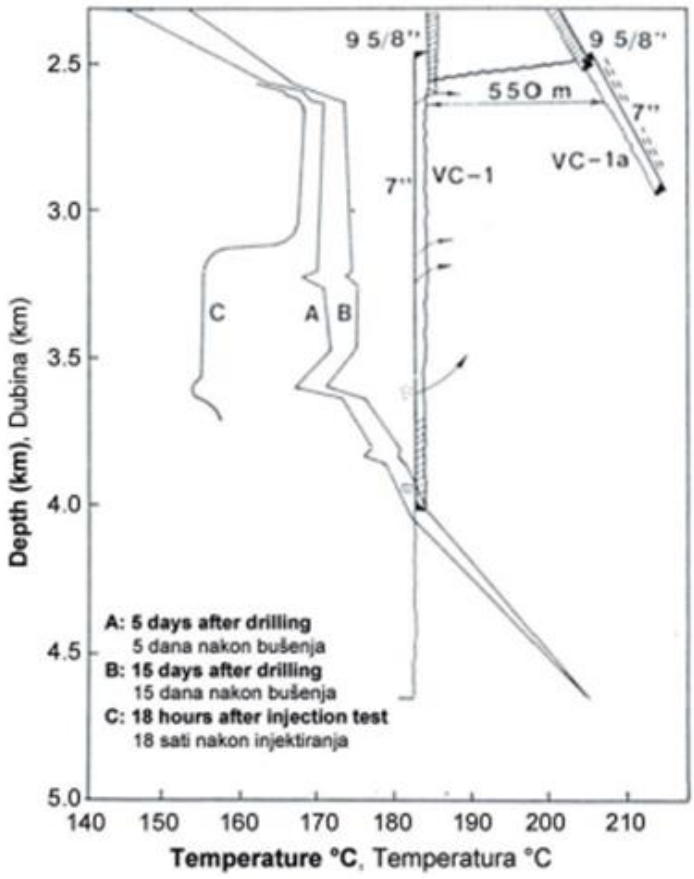

Figure 11: Well temperature profiles at the Ciglena geothermal power plan (Croatia)

Velika 1 power plant uses organic Rankine cycle to produce electrical energy. The installed capacity is 16.5 MW, but the net power is 10 MW according to the contract with Croatia electricity regulator. The working fluid is isobutane and the cooling system is an air cooled condenser. The geothermal water is at temperature 166 °C, and pressure 30 bar. The volumetric flow rate is 800 m^3/h. The outlet temperature of the water from the heat exchanger is 75 °C.

Figure 12: ISP students at the Ciglena geothermal power plan (Croatia)

This power plant was visited on April 26th 2022 by ISP students and accompanying staff members (Figure 12).

References

Albert Genter, Keith Evans, Nicolas Cuenot, Daniel Fritsch, Bernard Sanjuan. Contribution of the exploration of deep crystalline fractured reservoir of Soultz to the knowledge of enhanced geothermal systems (EGS). Comptes Rendus Geoscience,Volume 342, Issues 7–8, 2010, Pages 502-516,ISSN 1631-0713.

2.2.3 Geothermal exploitation sites within an oceanic rift area

The Hengill system is part of the wider Hengill region, which covers 112 square kilometres in southwest Iceland (Figure 13). It is one of the most extensive geothermal areas in Iceland. The Hengill central volcano is still active, even though the last eruption occurred 2 000 years ago. The volcano has erupted 3 times since last ice age (9000, 5000 and 2000 years ago). Gasperikova, 2015 describe that the Hengill geothermal system is formed by the percolation of groundwater from the heat source at the base of the central volcano. The geothermal fluid is subsequently moving toward

SW and NE along the dykes and fissures. Like that the Hellisheidi and Nesjavellir geothermal systems are fed. The permeability along the dykes and fissures is very good, which are the main drilling target. The temperature of reservoir ranges from 200 up to 340°C. The conceptual model of the Hengill geothermal system was described by (Franzson, 2010).

There are 2 geothermal power plants on the Hengill system; the Hellisheiði power plant generates 303 MW_e* and 133 MW_{th}, and the Nesjavellir power plant generating 130 MW_e and 290 MW_{th} (all the MW_{th} is for the district heating in Reykjavik).

Reykjavík Energy is the one company who holds right to explore this area. The company drilled 55 production wells, 17 reinjection wells and five make-up wells in the Hengill Area between the years 2001–2011. Most of the wells were drilled with modern drilling rigs, up to four simultaneously, all-hydraulic with a top-drive and the large ones with automatic pipe handling (Sveinbjornsson, 2014). Sveinbjornsson and Thorhallsson (2014) stated that for geothermal power projects about 40–50% of the total investment cost lies in drilling of the production and reinjection wells and construction of the steam supply system for the plant.

The production density at Hellisheiði is 14 MW_e/km^2 and Nesjavellir is 15MW_e/km^2. MW_e is Megawatts of electricity, and MW_{th} is megawatts of thermal energy.

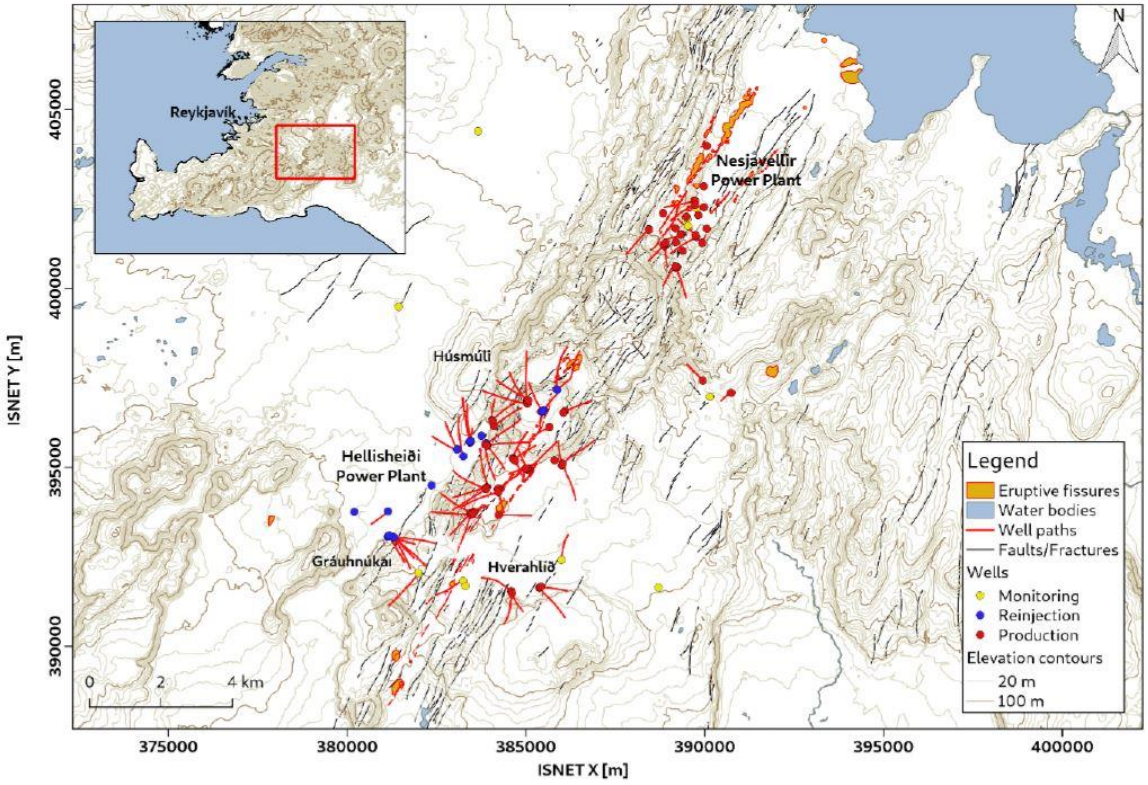

Figure 13: Map of Hengill area showing surface contours, eruptive fissures and mapped fractures. Well tracks are shown in red. From Gunnarsson et al, 2021.

On June 21st 2022, ISP students and accompanying staff had the opportunity to visit the Hellisheidi power plant and get insights on ORC technology (Figure 14).

Figure 14 ORC view at Hellisheidi powerplant

References

Franzson, H. E. (2010). The Hengill Geothermal System, Conceptual Model and Thermal Evolution. Proceedings World Geothermal Congress.

Gasperikova, E. G. (2015). Resistivity Characterization of the Krafla and Hengill Geothermal Fields through 3D MT Inverse Modeling.". Geothermics, 246-257.

Gunnarsson, G. T. (2020+1). Managing the Production Fields in the Hengill Area. Proceedings World Geothermal Congress . Reykjavik.

Sveinbjornsson, B. M. (2014). Drilling Performance, Injectivity and Productivity of Geothermal Wells. Geothermics, 76-84.

Sveinbjornsson, B.M., Thorhallsson, S. (2014). Drilling performance, injectivity and productivity of geothermal wells, Geothermics,Volume 50, 76-84.

3 Geological excursions and data analysis on geothermal reservoir analogues

Reservoir exploration and understanding is a task of primary importance when planning geothermal energy utilization.

This task is challenging as reservoirs are buried sometimes at great depth where geological information is limited to a low number of expensive boreholes and indirect geophysical data. Whenever possible, reservoir engineers are using naturally exhumed paleo reservoirs in order to gain statistically representative data.

The main geological characteristics of the different visited provinces are now summarized.

3.1 Sedimentary basins

3.1.1 The Pannonian basin

Croatia is settled within two main regional geological provinces – Pannonian basin to the north, and Dinarides to the south (Figure 15). Both units are results of indentation of Ancient Ocean and their archipelagos backed by the African plate to the Euro-Asian plate bay, controlled by Check and Moesia massifs that started in Cretaceous. Today's geological setting in Croatia, was developed in several phases resulting in the rise of the main part of Dinaridic carbonate platform, with southwest verging foreland, mostly developed in the Adriatic offshore, backed by mountain belt extending in a northwest-southeast direction along with important strike-slip compensation. At the inner Pannonian side, north branch of Dinaridic carbonate platform's archipelagos are twisted around central Bosnian massifs and its fragments, by indentation entered deeply into the future basin area, even to the north and to the east of the Croatian Pannonian territory, forming the basin basement and marking the proto basin troughs initially filed with sin-orogenetic material.

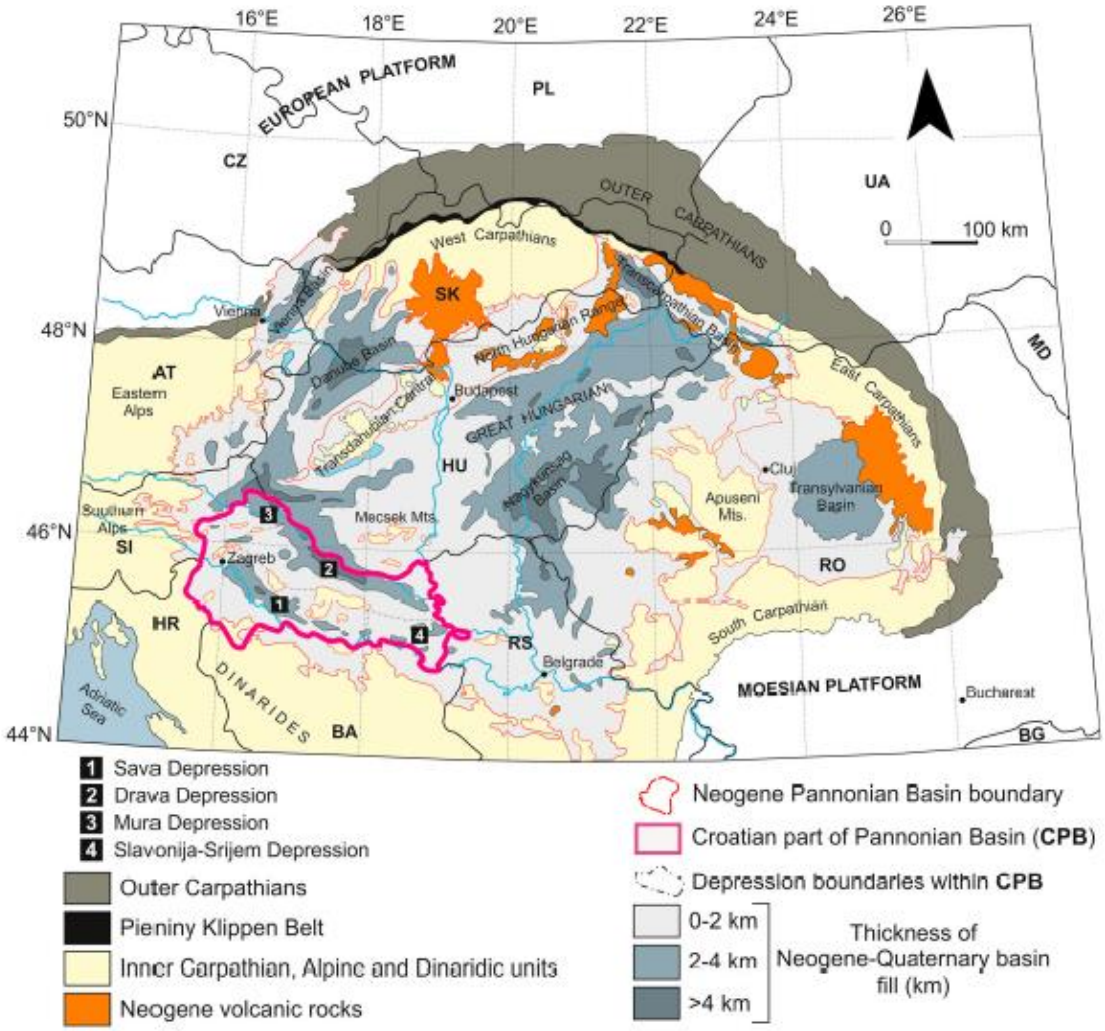

Figure 15: Map of principal tectonic and geographic units of the Alps, Carpathians, Dinarides and the Pannonian Basin with its subbasins and depocentres (Cvetković, 2019)

That rise of the main part of Dinarides was caused by subduction of the Adriatic plate and deepening of the Moho discontinuity to 35-40 km in the narrow northwest-southeast direction and consequently formation of a back-arc type basin in the Pannonian area. Future basin area was firstly characterized by uprising and thinning of the crust and differential erosion of sedimentary cover and opening of proto basins with local sedimentation, followed by isotactic subsidence in the mid-Miocene, finally setting Moho discontinuity in the Pannonian area at about 25-30 km (Figure 16).

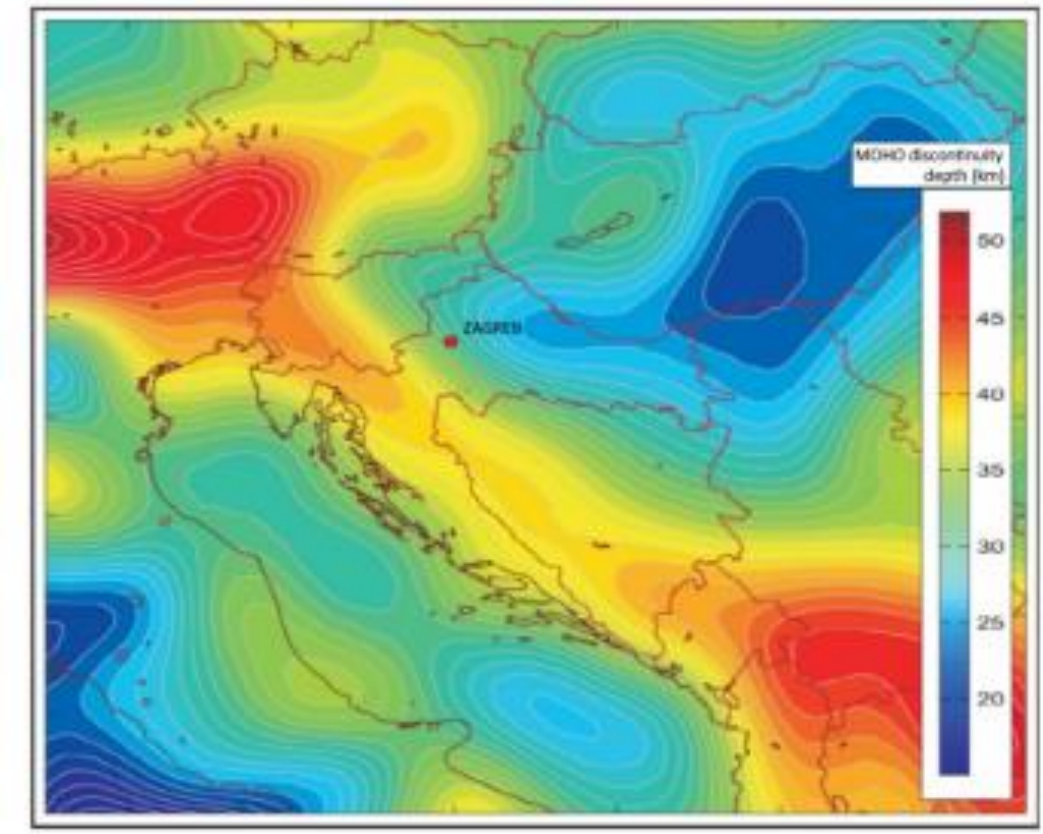

Figure 16: Map of Moho discontinuity depths in SE Europe (Grad et al. 2009)

Described geological features in the Pannonian area, such as crustal thickness, basin sedimentary cover and fragments of a massive carbonate platform sequences, control the geothermal features of the country in crustal and important deep water body settings (Kolbah, 2010)controlling geothermal surface flow by thermal conduction and convection models. The Pannonian basin area has a significant geothermal potential where the geothermal temperature gradient is commonly higher than 40°C/km and in top of important geothermal water bodies reaches values of more than 70°C/km. The terrestrial heat-flow density is also high, ranging from 60 to over 100 mW/m2 with an opportunity to find high-temperature water accumulations (Figure 17). Accordingly, along with hydro-geothermal resources, here we can also expect possible dry rock or enhanced geothermal energy resources.

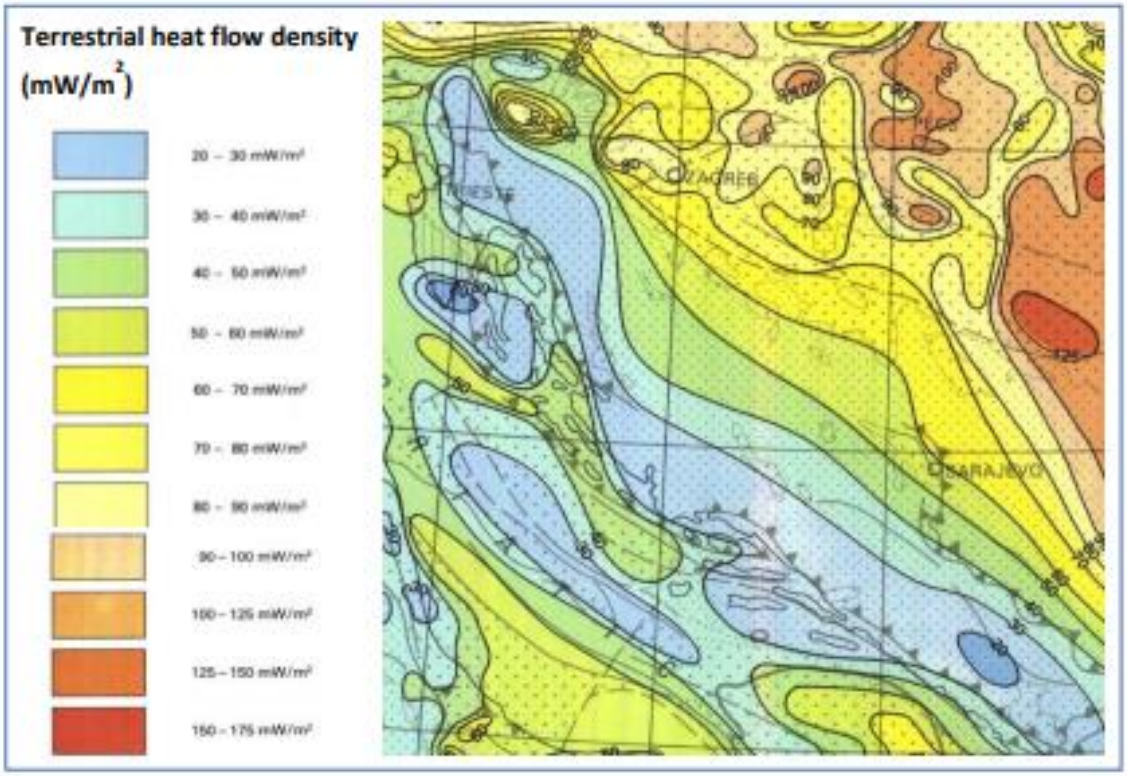

Figure 17: Terrestrial heat flow density in Croatia (Hurtig et al., 1992)

The geothermal potential of the Pannonian basin area is marked with 30 major natural springs of thermal water, many of which have been known since Roman times. They exhibit temperatures up to 65°C and have often been developed with wells to reach waters with higher temperatures or increase flow rates. Moreover, waters with higher water temperatures were found during oil and gas research taken in the Pannonian basin area in the second part of the 20th century. In that time, massive geological and geophysical exploration finalized with more than 4,000 deep wells drilled. Nearly fifty oil and gas fields and five geothermal fields (Elezović I., 2018) were put in production. There are two main types of geothermal aquifers: the one with intergranular porosity in clastic sediments of Mesozoic and Tertiary age and the other with secondary porosity - fractures and caverns of Mesozoic and Miocene carbonates. Mesozoic massive carbonate deposits with highly developed secondary porosity provide reservoirs with richer flows and higher formation temperatures such as Velika Ciglena (175°C) now in production, Kutnjak-Lunjkovec (140°C), and Slatina (190°C) with high production level favorable for electricity generation by modern technology and economy.

One of the main issues when working within the Pannonian basin is the scarcity of pedagogically relevant outcrops. Luckily, intensive oil prospection in the past century lead to a good geological understanding of the Croatian territory underground and numerous data in terms of geophysics and samples gained from borehole are now published.

Geological models reconstructions, data interpretation are thereofore available to students. Among the whole dataset the Geo3EN project has chosen two sites, namely the Velika Ciglena area and Zagreb geothermal field.

3.1.1.1 The Velika Ciglena project

The Velika Ciglena project area is located in the SW part of Pannonian basin, in the Bjelovar sub-depression, NE part of Croatia (Figure 18).

Figure 18: Croatian part of the Pannonian basin system

The latest structural and tectonic solution of the Velika Ciglena geothermal reservoir is shown schematically on the map (Figure 19), and on the longitudinal cross-section (Figure 20). A very similar disposition of faults was shown at that time, the only differences being distances between them. The later solution was affected by additional seismic measurements and the results of drilling of two (dry) exploratory oil wells (VC-2, Ptk-1).

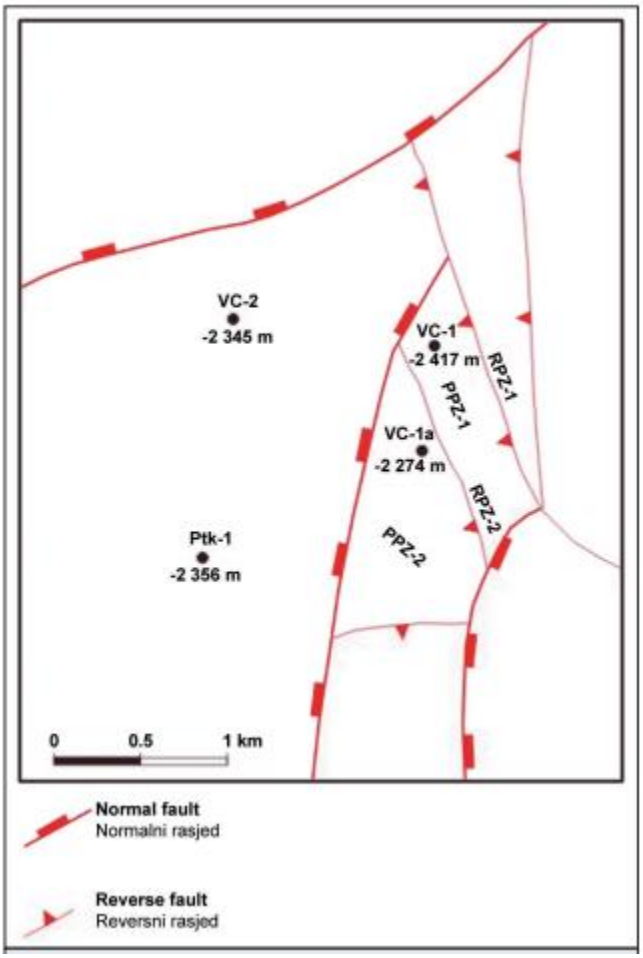

Figure 19: Tectonic map of the Velika Ciglena geothermal reservoir

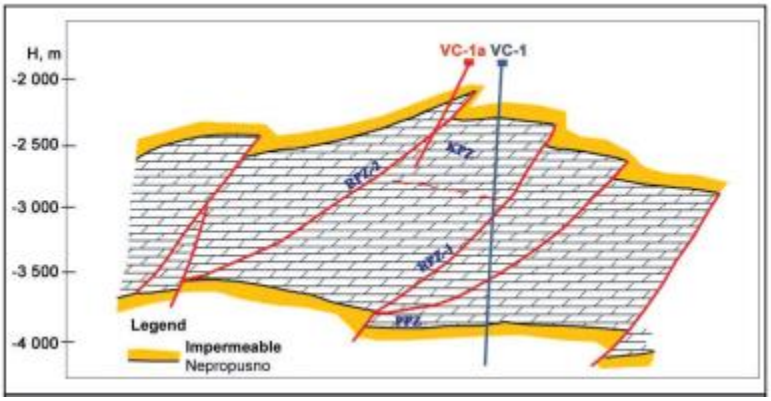

Figure 20: Longitudinal cross – section across the VC-1 and VC-1a wells

Those two wells penetrated only a small part of the geothermal reservoir thickness. Indirectly, it is evident from the high temperature and drilling fluid circulation losses that a geothermal reservoir of good flow properties was penetrated. Description of geological setting stresses that normal faults are probably barriers. Because of that, the new wells are probably not hydraulically connected with wells VC-1 and VC-1a.

3.1.1.2 The Zagreb Geothermal Field (ZGF)

The ZGF is a very suitable locality to test the methodologies and workflows to be established in the scope of reservoir model reconstruction by students.

As part of the hydrocarbon research in the 1960s, a geothermal aquifer with favorable properties was discovered. Unlike many other localities in the Croatian part of the Pannonian Basin System (PBS), this aquifer was not abandoned. Rather, the opportunity of using the resource was recognized and it was further developed as a geothermal field. Research and drilling continued until 1988. Although the boreholes in the external part of the field are also utilized (e.g. Lučanka and Nedelja boreholes), the main development is represented by two so called "technological systems": Mladost and KBNZ (in the central part of the field, with the highest measured temperatures and geothermal gradients).

Figure 21 shows the schematic cross-section of the ZGF area.

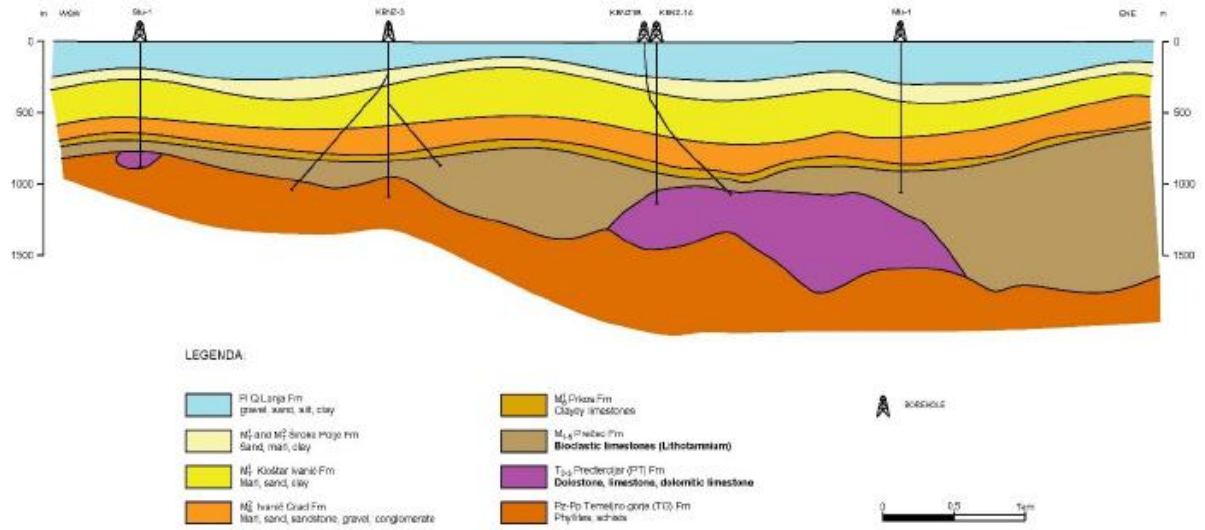

Figure 21: Schematic geological cross-section, redrawn according to Zelić et al. (1995)

The main geothermal aquifers, as identified in the existing boreholes are M1-5 Prečec Formation bioclastic (Lithotamnium) limestones and T2-3 Podloga tercijara (PT) Formation dolostones, limestones, and dolomitic limestones. They vary significantly in thickness in this small area: M1-5 from 35 m to greater than 1016 m and T2-3 from 5 m to 357 m. Lithothamnium limestones are characterized by primary and secondary porosity which results in good overall permeability. The Triassic carbonates have low matrix porosity so good permeability is attributed only to secondary porosity. Recorded water temperatures in the boreholes ranged from a minimum of 34 °C up to a maximum of 78 °C at the Mladost technological system and 82 °C in the KBNZ system.

In the majority of the boreholes, the formation yielding water is the Miocene bioclastic limestone. However, for practical purposes the two formations are considered as a single hydro-stratigraphic unit.

It can be seen in Figure 21 that no fault structures were defined, although the cross-section is from the main mining design of the ZGF (Zelić, 1995) and declaratively it is based on both borehole data and interpretation of seismic cross-sections. However, initial analyses of seismic cross-sections clearly indicate the presence of fault structures. This is the part of the conceptual model which obviously needs to be revised, and students can elaborate their own 3D interpretation using numerical tools as presented in Figure 22. An upcoming task is to make a combined interpretation of seismic reflection and borehole data (converted to time domain), and then perform a conversion of the interpreted cross-sections back to the depth domain. Also, it is important to input borehole inclination azimuths and make corrections of thermal log data, to get a more realistic representation of temperatures at true vertical depths.

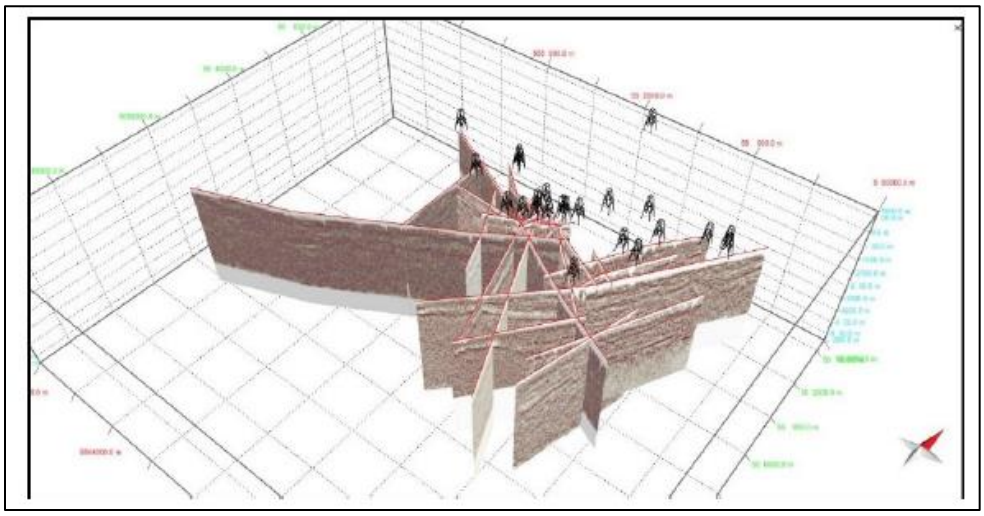

Figure 22: Project of seismic and borehole data in the MOVE software by Borović et al (2021)

Seismic and borehole data will be used to perform a 3D geological reconstruction of the subsurface and to highlight the principal fault systems. The 3D geological model will be used to numerically reconstruct the subsurface thermal regime. Coupled fluid flow and heat transport numerical simulations will be performed using data on the hydrodynamic and thermal properties of the formations. First, the simulations will be run at steady state to assess the contribution of conductive processes to the thermal regime. Further transient simulations will be performed to evaluate the impact of the (most likely convective) processes occurring in the fractured carbonate reservoir and contributing to the local temperature increase. The obtained results of temperature model will be compared and calibrated with available bottom hole temperatures and thermal logs.

References

Borović, S., Pola, M., Pavičić, I., Špelić, M. Utilization of Vintage Hydrocarbon Exploration Data in Geothermal Research: the Case Study of Zagreb Geothermal Field (Croatia). Proceedings World Geothermal Congress 2020+1 Reykjavik, Iceland, April - October 2021

Cvetković, M., Matoš, B., Rukavina, D., Kolenković Močilac, I., Saftić, B., Baketarić, T., Baketarić, M., Vuić, I., Stopar, A., Jarić A., Paškov, T. Geoenergy potential of the Croatian part of Pannonian Basin:

insights from the reconstruction of the pre-Neogene basement unconformity. Journal of maps 2019, Vol. 15, No. 2, 651–661 https://doi.org/10.1080/17445647.2019.1645052
Elezović I., Škrlec M. & Kolbah S.: Construction of Wells for Geothermal Production in Croatia, HUNIG Zagreb, *Nafta i Plin bulletin*, Vol. 38., No. 155 (2018).
Grad M., Tiira T., ESC Working Group, 2009. The Moho depth map of the European Plate. *Geophys. J. Int.*, 176, 279–292, doi: 10.1111/j.1365-246X.2008.03919.x
Hurtig, E., Čermak. V., Haenel, R. and Zui, V.: Geothermal atlas of Europe, Working group „Geothermal atlas of Europe" of the International Heat Flow Commission (Yugoslavia: D. Ravnik, S. Kolbah, K. Jelić, M. Milovanović, N. Miošić, S. Tomić, D. Rajver; 102-105), Kartographisher Dienst Potsdam, Hermann Haack Verlagesgesellschaft mbH Gotha, Germany, (1992).
Kolbah, S.: Deep Transboundary Water-Bodies: Exploration and Management in the Pannonian Basin of the Republic of Croatia, *Proceedings*, UNESCO-IAH-UNEP Conference, Paris, France, p. 6-8 (2010).
Virkir Orkint Consulting Group Ltd, Iceland: Pre-Feasibility report of Geo - thermal development for combined electricity and heat production in Croatia, 1995.
Zelić, M., Čubrić, S., Kulenović, I., Kušek, M., Marčan, B. et al.: Main mining design of the Zagreb Geothermal Field. INA plc., Zagreb, (1995), 268 p. (in Croatian)

3.1.2 The Aquitaine Basin

As in the Pannonian Basin the scarcity of outcrops in the Aquitaine Basin complicates teaching activities on geothermal analogues.

A two days field excursion also the Atlantic coast about 85 km NNW from Bordeaux city by members from TU Darmstadt and UniLaSalle permitted to find at Plage de Gurp (Figure 23) an exceptional outcrop exposure to be used in terms of subsurface fluid flows. The system is considered as an easy to reach analogue of a shallow geothermal system.

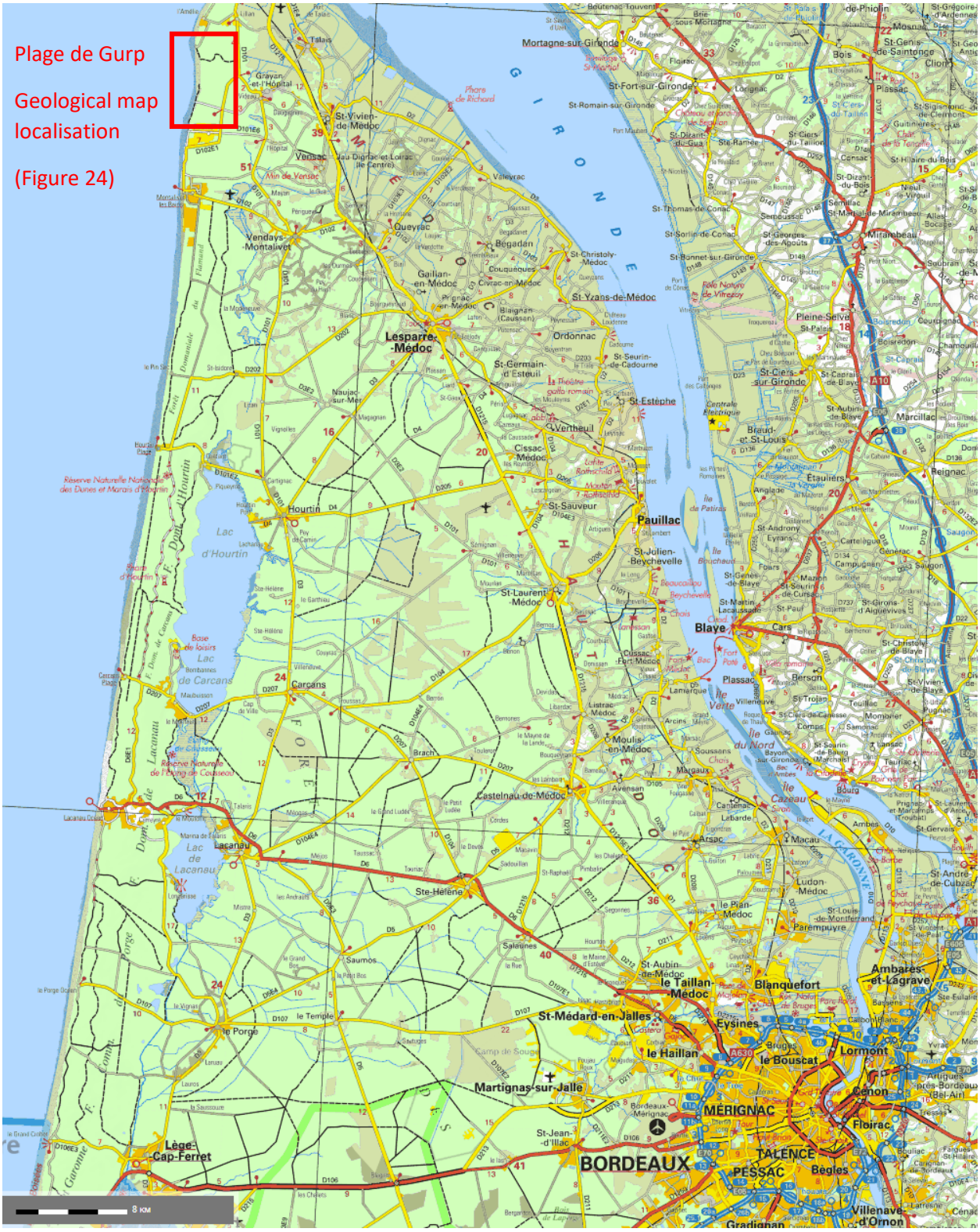

Figure 23: Localisation of Plage de Gurp

According to information found in the litterature, namely BRGM geological map (Figure 24) and accompanying cross section (Figure 25) the geological units consist in

- An Oligocene basement of about three meters consisting of marls at the base of the unit and limestones at the top (g2)
- Pleistocene units
- Pre Mindel and Mindel units (Fu) consisting of gravels at the base and pebbles at the top
- Interglacial Mindel Riss (Fv) mainly consisting of clays (Gurp clays unit)
- Würm 3 and Würm 4 (Fw) consisting of coarse fluvial sands (Gurp fluvial sands unit)
- Holocene
- Paleo dunes (Dya and Dyb)
- Present day dunes (Dz)

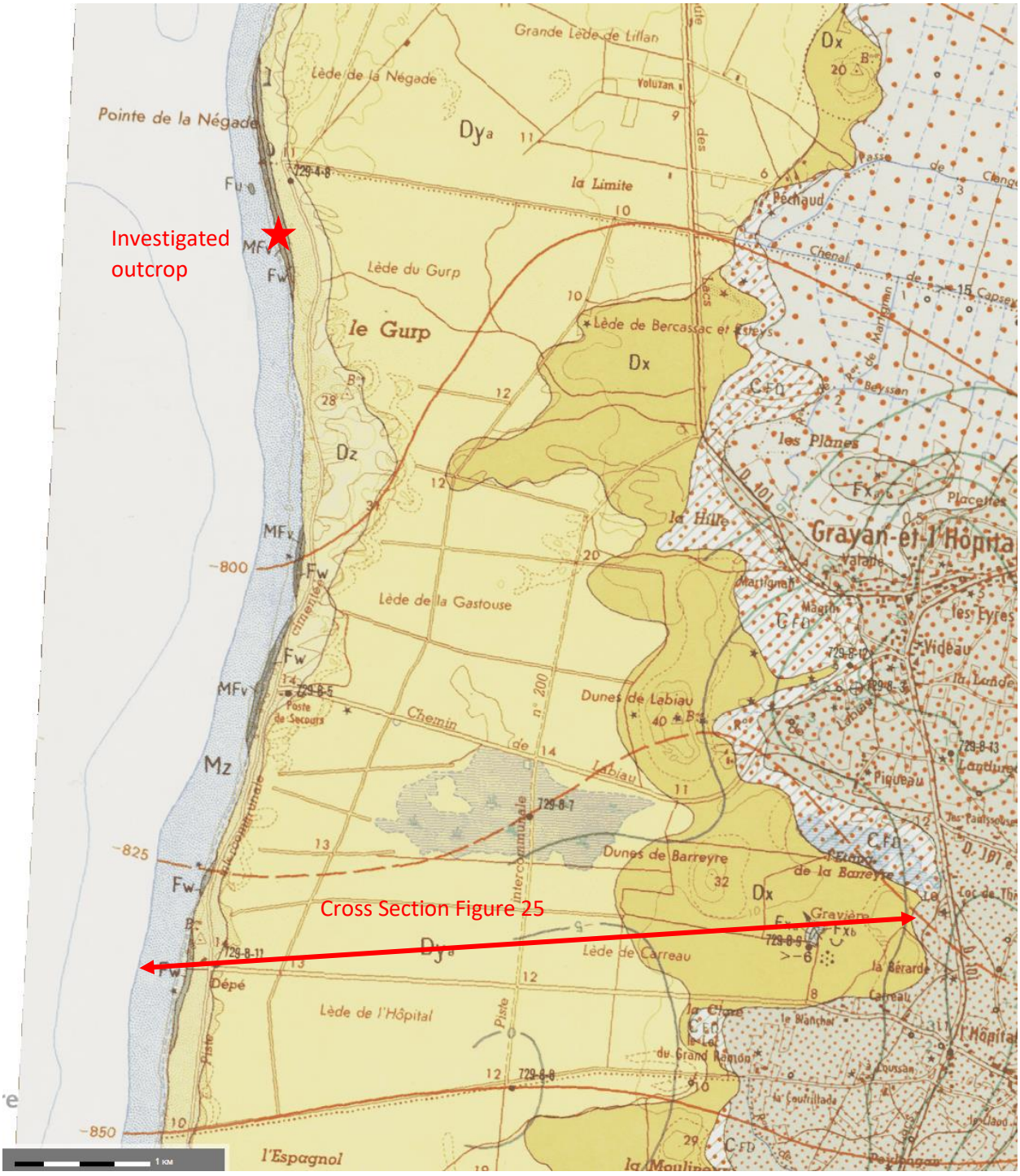

Figure 24: Geological map of plage de Gurp area. See figure for legend. BRGM geological map St Vivien de Médoc / Soulac sur Mer XIV - 33

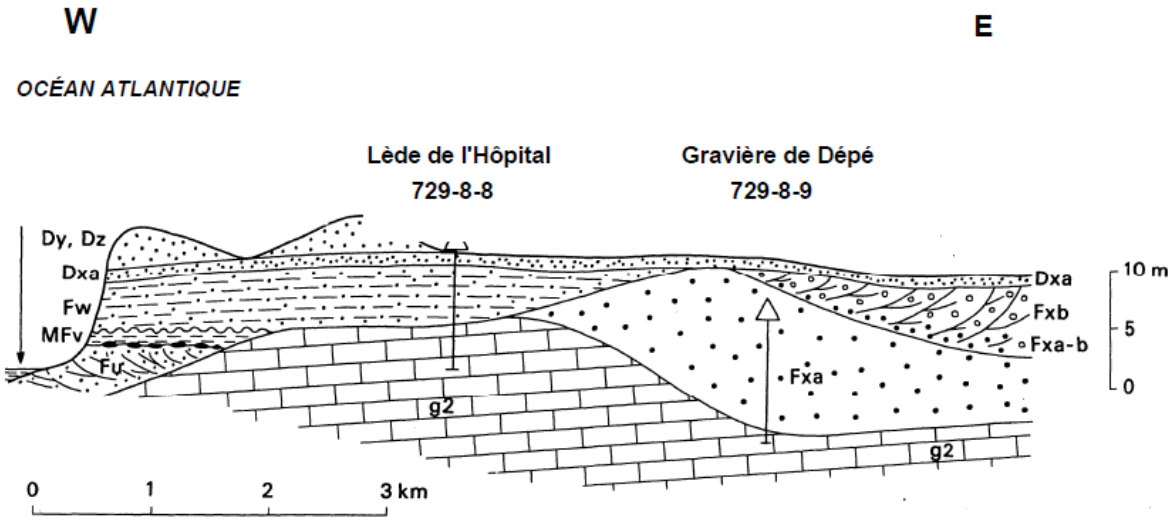

Figure 25: Glacial period deposits interpretation. Geological cross section, see map trace in figure 26

Dz, Dy, Dxb, Dxa: Post glacial eolian formations

Fxb: Méric formation

Fxa: Dépé formation

Fw: Gurp fluviatile sands

MFv: Gurp clays

Fu: Négade formation

g2: Bed Rock (Stampian)

The outcrop consists in two layers of consolidated organic material, metric in scale, interlayered with compacted sand deposits. This alternance is buried under the present day dune and outcrops directly along the beach (Figure 26 and Figure 27). Behind the present day dune, a paleo dune system can be observed, forming a basin tilted towards the ocean (Figure 28).

This outcrop is of particular interest as it represents an easy to reach shallow geothermal reservoir analogue. Understanding fluid circulations in layered, non isotropic reservoirs are of primary concern for engineers and the present outcrop represents an exceptional study object from a pedagogical perspective.

Figure 26: Panoramic view of the investigated outcrop

Figure 27: Close up on the stratigraphic succession consisting in two impermeable organic rich layers from the Gurp formation.

E W

Figure 28: Panoramic view of the dune system overlying the investigated outcrop

In spite of a serious drought having affected he whole Aquitaine basin for several months before the visit, a permanent fresh water flow, non-salty oceanic water rich in iron oxydes and possibly magnesium sulfates is observed at the top of both organic rich layers. These streams of water are running down on the beach and are outlined by streaks of iron oxydes precipitates visible on several tens of meters along the beach, down to the ocean. No fresh water is percolating through the sand layers, and all flow occurs at the interface between sand and organic layer.

The origin of this fresh water is at present a matter of debate. It is thinkable that a fresh water aquifer is being dragged at the top or impermeable layers by a complex interplay between reservoir anisotropy, layer tilting and hydrostatic pressure related to Atlantic Ocean tides.

In any case, the analogue permits to map the lateral continuity of the drainage area and establish an hydrological flow model. Activities like drone assisted LIDAR mapping, ground photogrammetry, stratigraphic log profiling are immediately achievable in the field. Petrographical and petrophysical

investigation in terms of microfacies and grain size analyses, organic material maturity, porosity and permeability are immediately possible in the laboratories at TU Darmstadt and UniLaSalle. Carbon isotopes analysis and water composition determination are also feasible.

We expect that a one-week fieldtrip in the area followed by a similar duration laboratory practice will offer students a great opportunity to be trained in the field of hydrology and shallow geothermal systems.

References

BRGM geological map St Vivien de Médoc / Soulac sur Mer XIV – 33

3.2 Rift type basins with fractured basement rocks

The Upper Rhine Graben (URG) forms the central, most conspicuous segment of the ECRIS (Illies, 1965), which extends over a distance of more than 1000 km from the North Sea to the Mediterranean (Figure 29 and Figure 30). The NNE-trending URG, which is limited by the Rhenish Massif to the north and the Jura Mountains to the south, has a length of some 300 km and a width of 30–40 km. This geological setting will focus on the structural inheritance of the crystalline basement and the evolution of fractured system from Variscan to late Alpine. The Variscan crystalline basement of the URG is characterized by three major tectonic terranes, oriented NE to NNE, from north to south, the Rhenohercynian, the Saxothuringian and the Moldanubian that present major lithological differences ((Edel 2009); (Edel J. W., 1995); (Ziegler, 1990). They are intruded by carboniferous granitoid (340 Ma (Visean) and 270 Ma (Permian)) that exhibit a large petrological and geochemical diversity of crystalline rocks, which are related to a variety of active deep magmatic sources and different petrogenetic mechanisms ((Altherr, 2000), (1999); (Edel J.-B. S., 2009); (Lagarde, 1992). These granitoids are emplaced following a NE to NNE direction according to main weakness zones such as collisional or shear zones. These inherited Hercynian NE to NNE-striking crustal weakness were reactivated to the URG formation under compressional stresses during Alpine and Pyrenean collisions (Dèzes, 2004); (Edel J.-B. S., 2007); (Illies, 1972, 1965); (Schumacher, 2002); (Villemin, 1987). Mesozoic platform sediments of Triassic (Buntsandstein, Muschelkalk and Keuper) and Jurassic (Lias and Dogger) times that results from eroded Variscan belt are also affected by structural evolution during Cenozoic rifting. Villemin (1987) and Schumacher (2002) proposed a Cenozoic rifting of the URG divided into four brittle deformation phases, which were accompanied by different stress regimes from the late Eocene rifting to the late Miocene. The first phase (middle to late Eocene) was characterized by an N–S compressive regime. During the second phase (late Eocene to late Oligocene), major E–W extension resulted in the greatest rifting and the development of thick sedimentary sequences in the URG (Doebl, 1967). These events included two marine transgressions, which induced the deposition of the carbon-rich Pechelbronn layers and salt layers in the southern area of the graben, among others. During the early Miocene, the stress regime changed to an NE–SW-oriented compressive phase. This episode was characterized by the uplift of the upper mantle and crust, as suggested by the up-doming Moho and the beginning of volcanism at the Vogelsberg and Kaiserstuhl volcanos (Fuchs, 1987). The prevailing stress regime in the URG from the late Miocene to the present has been a compressional regime with an NW–SE orientation, as observed over much of central Europe, which resulted in a left-lateral transcurrent motion (Bergerat, 1985); (Illies H. G., 1979).

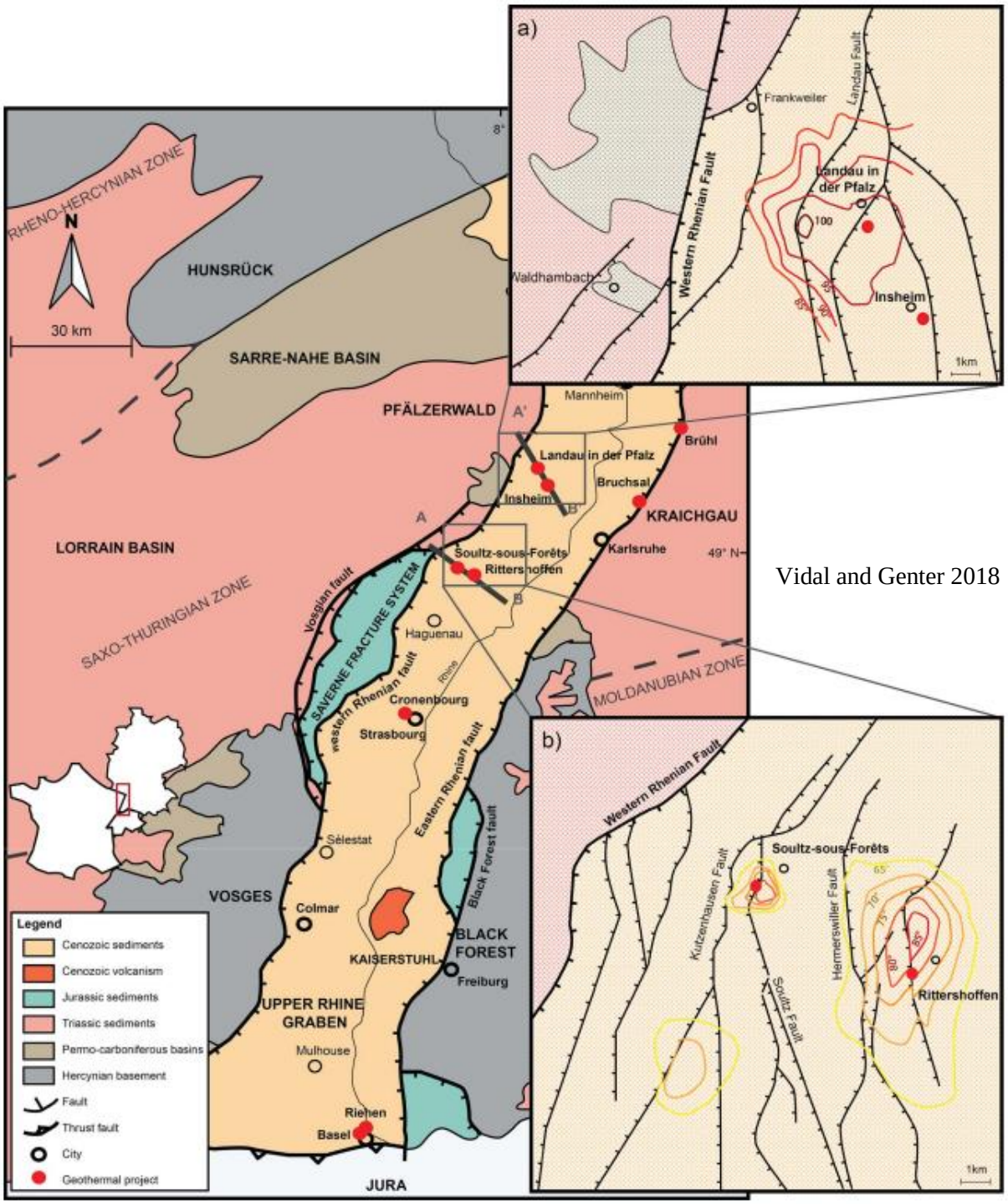

Vidal and Genter 2018

Figure 29: a) Simplified geological map of the Upper Rhine Graben and surrounding low mountain ranges, as well as basins including structural settings of selected high temperature areas of b) Soultz sous Forêts and Rittershoffen and c) Landau and Insheim.

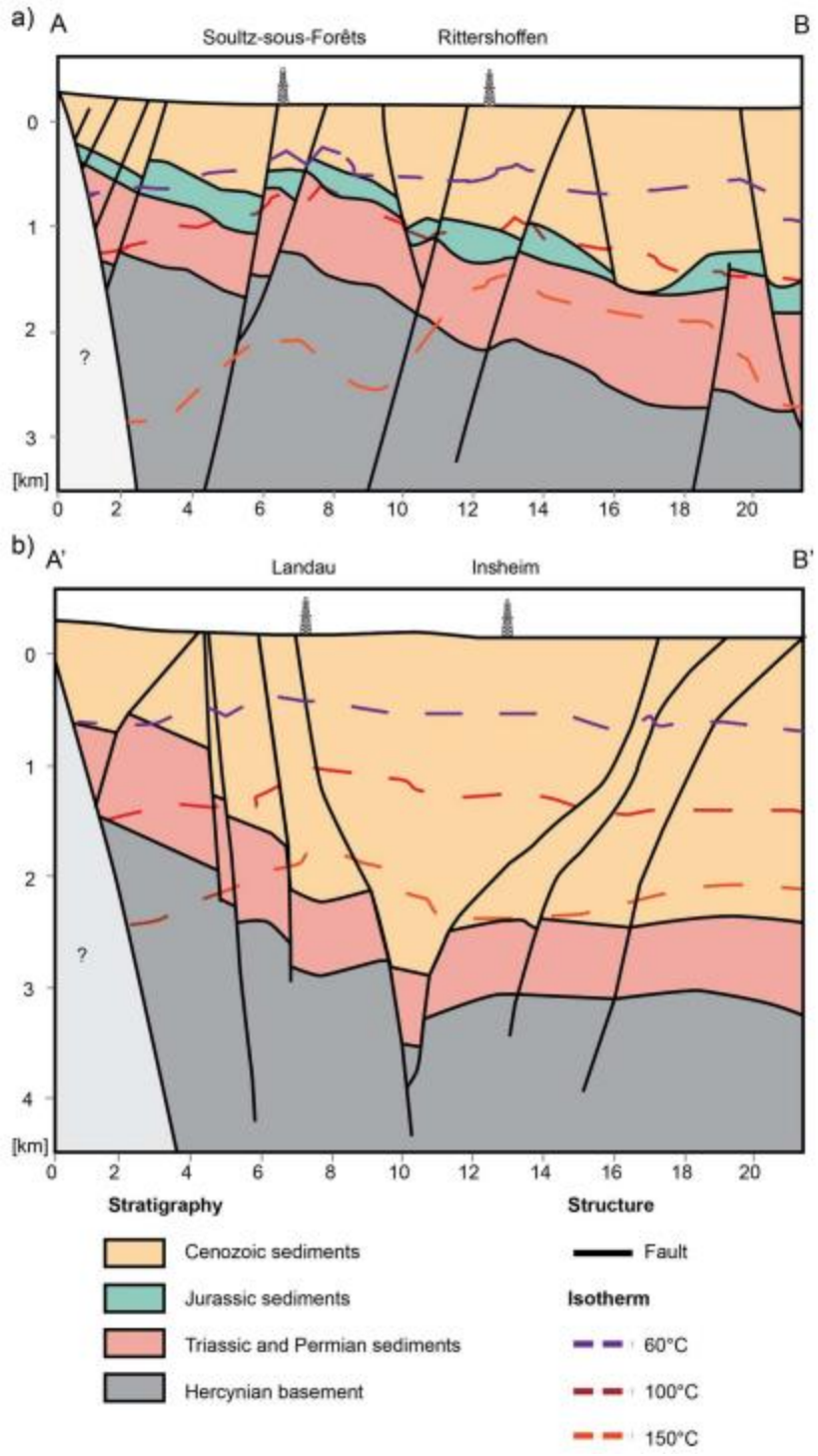

Figure 30: Simplified geological cross sections and isotherms obtained from geostatistical modeling across Soultz and Rittershoffen geothermal fields (AB in Figure) and across Landau and Insheim geothermal fields (A'B') in Figure 31

In the framework of the Geo3EN ISP program several reservoir analogues have been visited in the URG border massifs, namely in the Black Forest and Vosges. The excursion lead by UniLaSalle consisted in a

transect across the graben including a visit at Kaiserstuhl massif (Figure 31) and several paleo reservoirs consisting in hydrothermal ore deposits have been investigated.

Figure 31: ISP students at the Kaiserstuhl summit, at the Rhine Graben center. Panorama analysis.

3.2.1 The Gabe Gottes Mine in the Vosges moutains (Alsace, France)

Gabes Gottes mines is located next to Sainte-Marie-aux-Mines in France in the Vosges massif. The Vosges massif, being one of the URG shoulders, were subject to a several stress state changes through the geological periods (Figure 32). Distension and compression events occurred in the Carboniferous, the Permian was a distension period with different orientation of the minimum stress applied. In the Upper Eocene, a N-S compression took place. The Oligocene corresponds to the opening phase of the Rhine Graben. In the Miocene, the Vosges mountains were subject to compression.

The Gabe Gottes mine was exploited from the 10th to the 20th century for various ore minerals, and native silver. The mineralized veins occur in the “Varied gneiss group” which is composed of various lithologies including “pearl” gneiss, migmatitic gneiss and garnet gneiss locally intercalated with amphibolite and limestone (Hafeznia et al., 2015).

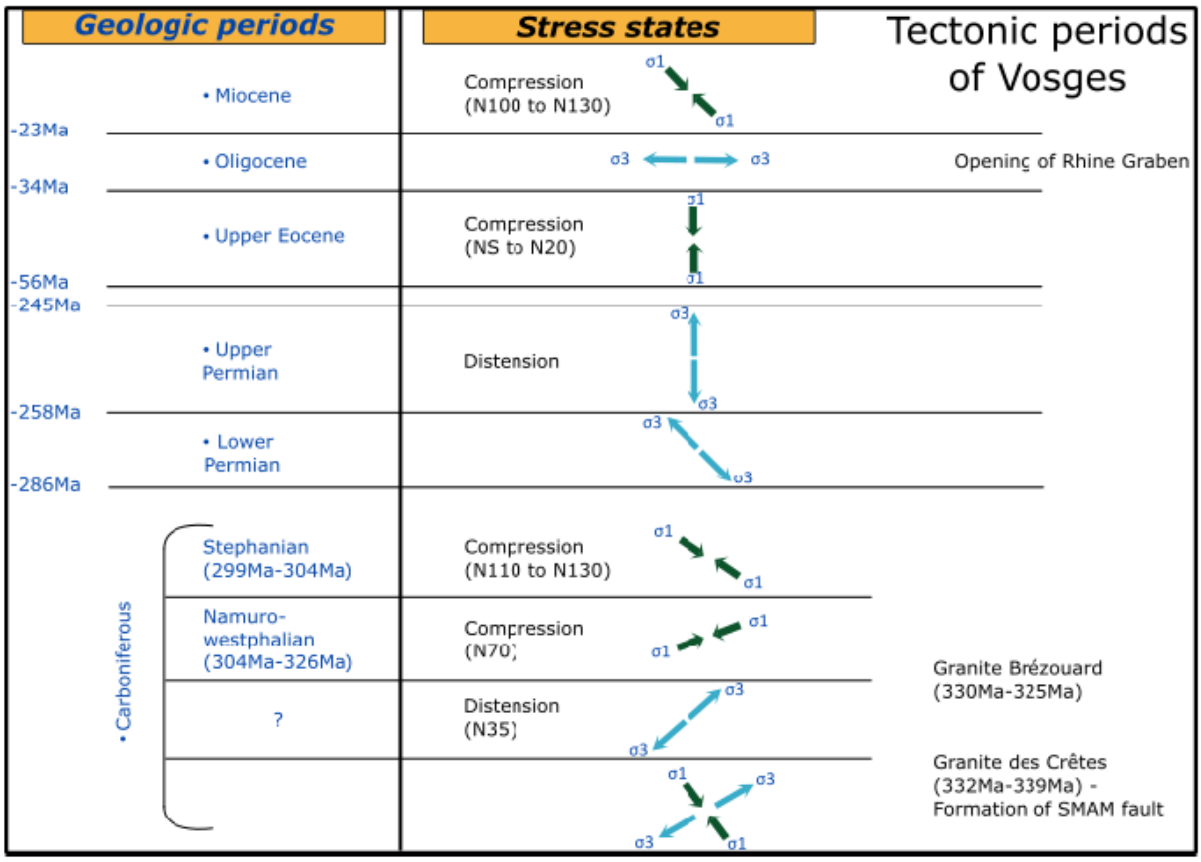

Figure 32: Tectonic phases of the Vosges mountains since the Carboniferous to the end of the Miocene (Hafeznia et al. 2015)

During the investigation, a focus was made on the P-west gallery (Figure 33). In this gallery was observed a highly deformed subvertical fault zone (Figure 34). This fault zone corresponds to a dextral shear zone with an E-W orientation (the Saint-Jacques fault system, Figure 33) which can be followed along the gallery. The shear zone appears highly deformed with stretched and boudinated basement rock elements preferentially orientated parallel to schistosity. Numerous movement indicators in the form of striations, mineral lineations and slickenslides confirm the transcurrent nature of this deformation zone ((Hafeznia, 2015) and own data).

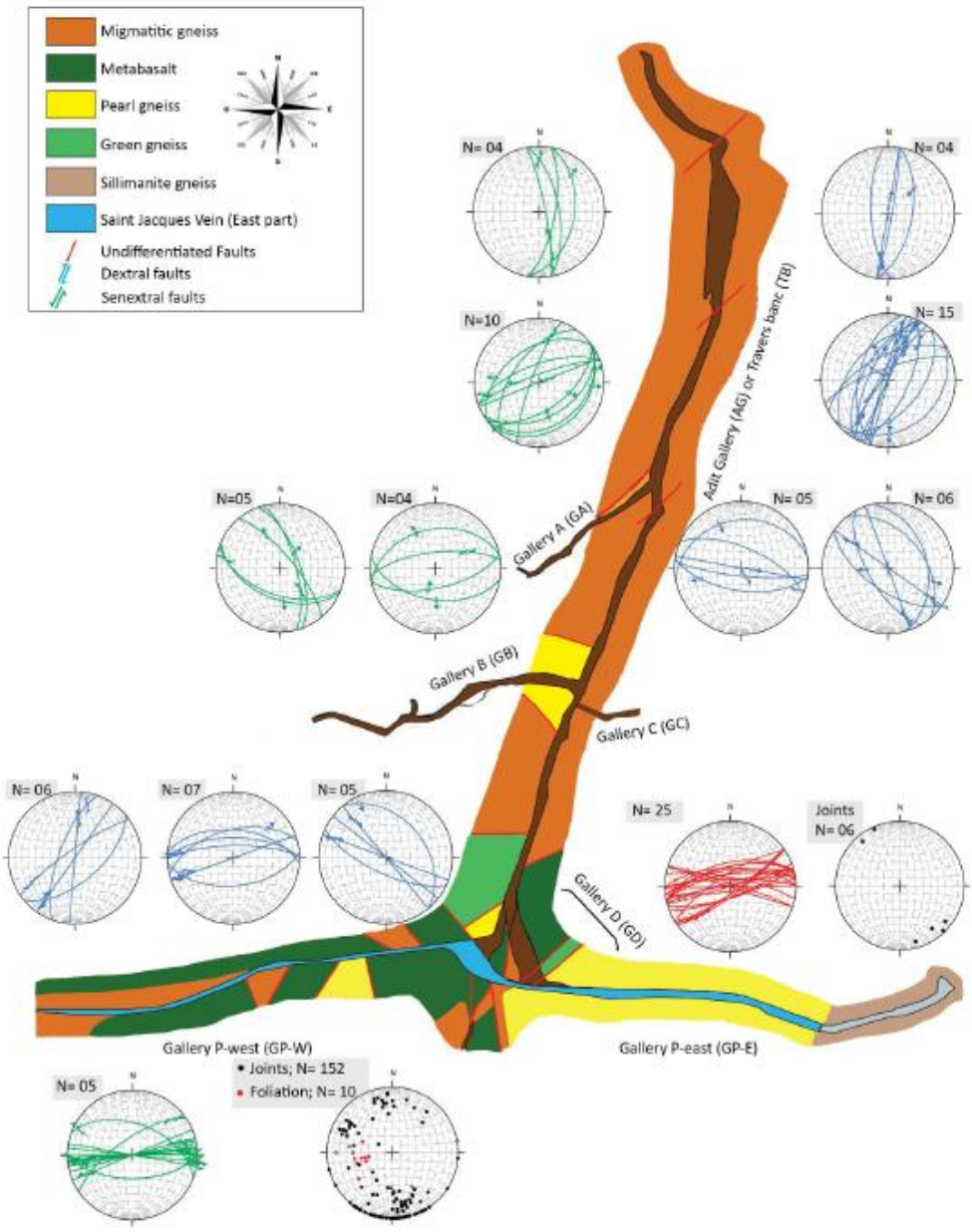

Figure 33: Geological map of the Gabe Gottes mine with fault analysis data

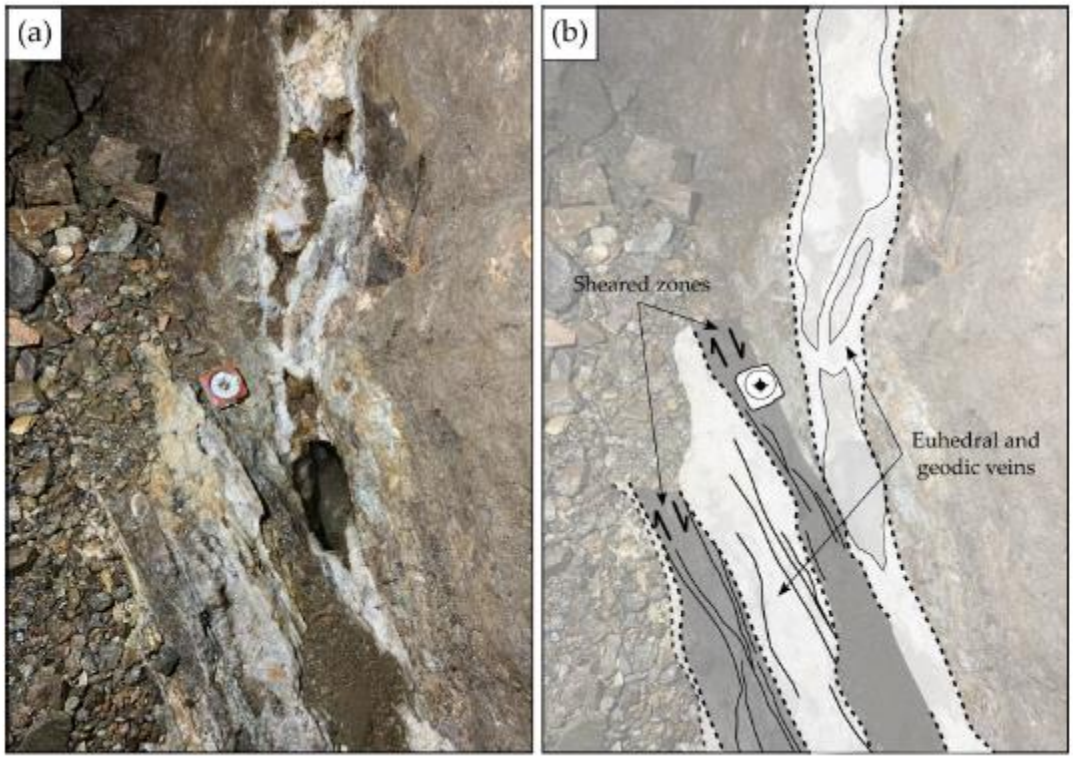

Figure 34: Interaction between a sheared zone and euhedral – geodic veins

The shear zone is interlayered with euhedral quartz veins of various width. Thinner veins were developed through these plans. Between these veins, veinlets crosscut the sheared zone making bridges between the larger veins. The interlayered veins are connected to wider vein orientated NW-SE found in the walls of the gallery. None of these veins present any sign of deformation meaning that the outcrop is misleading. In the case of a vein offset by a strike-slip shear zone, its infill should have been deformed. However, the vein infills are automorph and do not present any signs of stretching. The strike slip fault zone must preexist before the vein formation, a feature independently confirmed by isotopic dating and considerations of regional geology. By following the wide vein on the gallery wall along the shear zone, it is observed that its direction is changing from NW-SE to E-W.

The vein observed in the gallery wall is originally orientated NW-SE and changes its orientation when encountering the sheared zone. The strike slip shear zone which was created before the vein development, induce an anisotropy in the form of a schistosity within the host rock. This schistosity is predominant along the inherited deformation zone but vanishes quickly when moving away from it.
Pronounced rock alteration within the strike slip zone changes their mechanical response to loading. Alteration drastically influences initial rock competence and occurrence of a clear brittle failure becomes less obvious as a component of rock bulk creeping can be expected (Genevois, 1979). In addition, the earlier shistosity offers a preferential path to late fluid circulation.

It is proposed that the fluids circulating during the ore emplacement episode are deviated since fluid channeling along the planes of shistosity is easier then propagating a fracture across altered rocks.

3.2.2 The Teufelsgrund and Schauinsland mines (Black Forest, Germany)

The other place of interest which was investigated is the Schauinsland mine (10km SE of Freiburg im Breisgau, Germany), located in the Black Forest mountain (Figure 35). The Black Forest corresponds to the Eastern shoulder of the URG. Its western border is delimited by a major normal fault with a NNE-SSW orientation (Figure 35). The mountain is mostly made of crystalline granitic basement rock as in the Vosges Mountain. The structure is covered by Cenozoic and Mesozoic sedimentary rocks on its Eastern part (Werner, 2004).

The Schauinsland mine was exploited from the 13th century to the 20th for Lead (galena), zinc (sphalerite) and native silver. The Schauinsland massif is made of Pre-Cambrian crystalline basement rocks with different compositions and a lot of mineral veins were found. The ore mineral can reach a thickness of several meters and present evidences of several brine circulation pulses (Figure 36). A high strain fault zone was studied in the mines with a well-developed core and damage zone containing abundant clay minerals deposit. This shear zones transects the whole set of exploited galleries (Figure 36) and has been given the name Schuhmachersche Ruschel by miners. Isotope dating ((Werner, 2002) and references therein) has shown multiple reactivation of this deformation zone, with a dominant activity phase during the Jurassic.

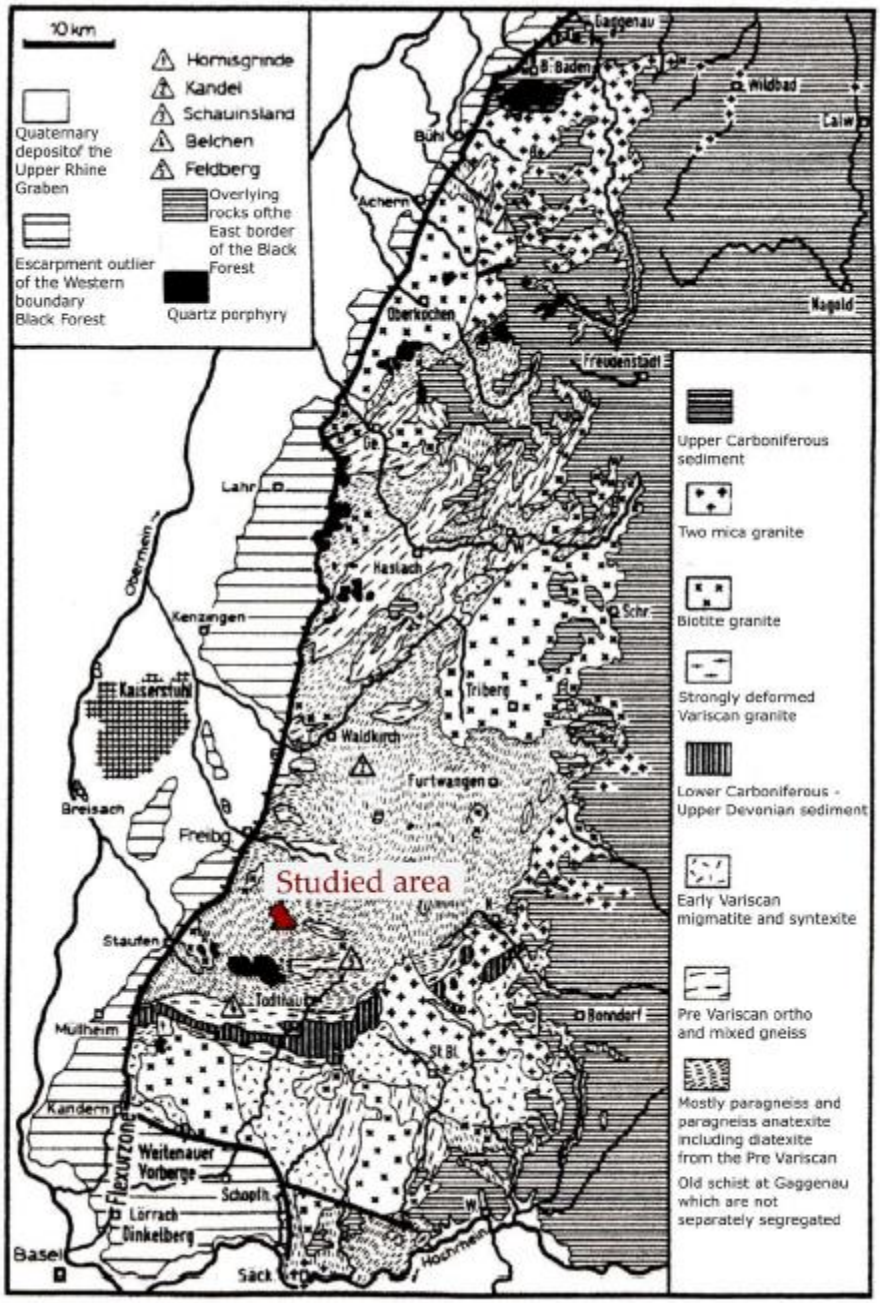

Figure 35: Geological map of the Black Forest. In red, the location of the detailed geological map of the Schauinsland area, translated after Wittenbrink (1999)

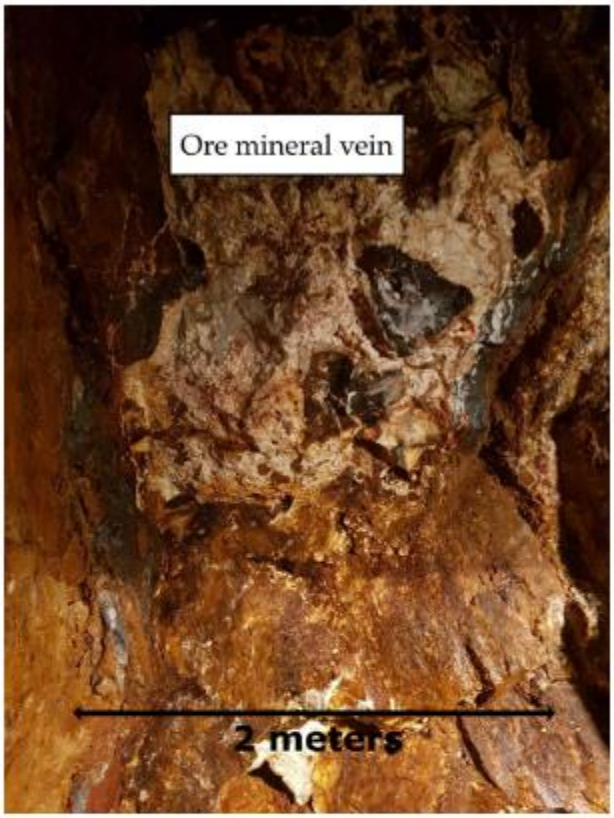

a)

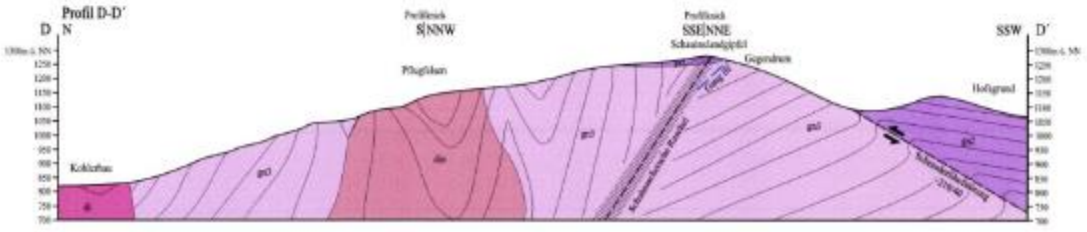

b)

Figure 36: a) ore mineral vein in Schauinsland showing evidence of brine circulation pulses, b) N-S cross-section of Schauinsland showing the Schumachersche Ruschel cross_cutting the massif, modified after Wittenbrink 1999

A profile study was made along the gallery (Figure 37 and Figure 38) where the highly sheared zone can be observed, the Schuhmachersche Ruschel (SR), presenting all the typical characteristics described by (Choi, 2016). At gallery entrance a pristine paragneiss and a vertical fault filled with baryte can be followed on the roof, following the gallery's orientation. The gallery was previously described by (Werner, 2004) where he documented the offset of a pre-existing high strain zone during a late phase of deformation responsible of ore mineral deposition (Figure 39). This chronology of polyphase deformation is confirmed by our observations. Evidences of clay smearing and ductile deformation features related to the SR offset are ubiquitous. The offset of the SR which is syn-kinematic to ore veins formation reworks an already

sheared clay rich fault core. This leads to spectacular, ductile driven, deformation features within the interference. The ore vein does not crosscut the SR zone and vanishes, it is only on the other side of the SR that the ore vein reappears.

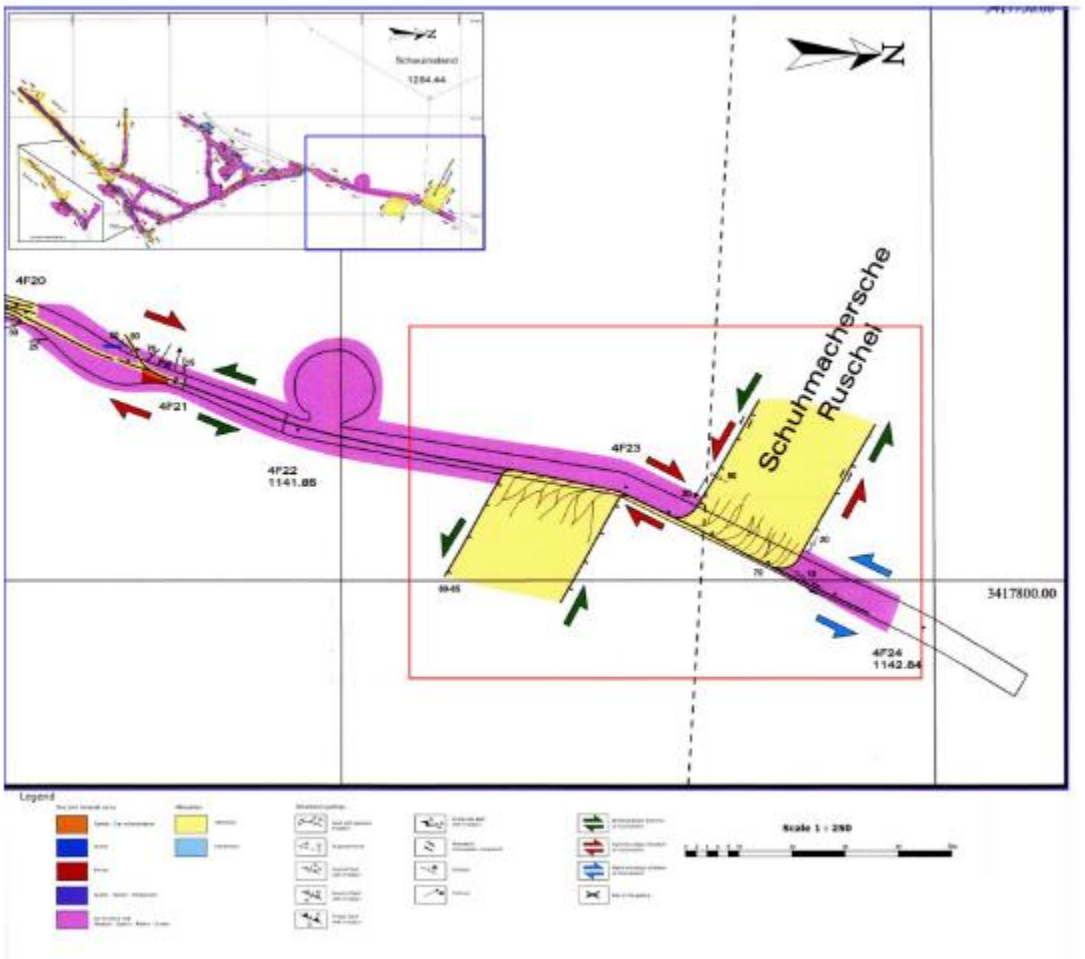

Figure 37: Geological map of the gallery, the studied area corresponds to the red rectangle where the beginning of the gallery is on the left, modified and translated after (Wittenbrink, 2002).

Figure 38: Photogrammetric model of the portion of the gallery showing the fault gouge

The observation that ore mineral veins well developed in unaltered host rocks wedge out in map view when approaching inherited high strain zone is of primary concern when dealing with late brine circulations in a pre-structured reservoir. The situation is comparable to present day geothermal saline fluids circulations within fractured basements.
The development of ore veins in basement rocks imply a sudden release of accumulated elastic stress in a competent unit. In the case of Schauinsland, the paragneiss can accumulate elastic stress. Fluid overpressures combined to a critically loaded rocks induce rock fracturing by cross cutting the Mohr Coulomb failure envelope. Failure leads to void opening in a transtensile regime and formation of breccia (sometimes hydraulic breccia) can occur.
The same coeval stress field being applied to a highly pre-structured shear zone rich in clay minerals (the SR zone) induces a drastically different mechanical response. Shearing is accommodated by plasticity, related to the increasing amount of inherited clay minerals. Clay plasticity driven mechanisms are progressively replacing brittle behavior when entering the inherited SR deformation zone. The brittle behavior is replaced due to inherited clay minerals and elastic stress can no longer be accumulated. Brittle failure of the host rock becomes more and more difficult.

The onset of plasticity plays a crucial role in development of late fluid flow paths, hindering accumulation of elastic stresses. Under these mechanical conditions, vein opening by sudden rock failure becomes impossible and channeled brine circulation can be stopped as in Schauinsland or decreased and deviated as in Gabe Gottes.

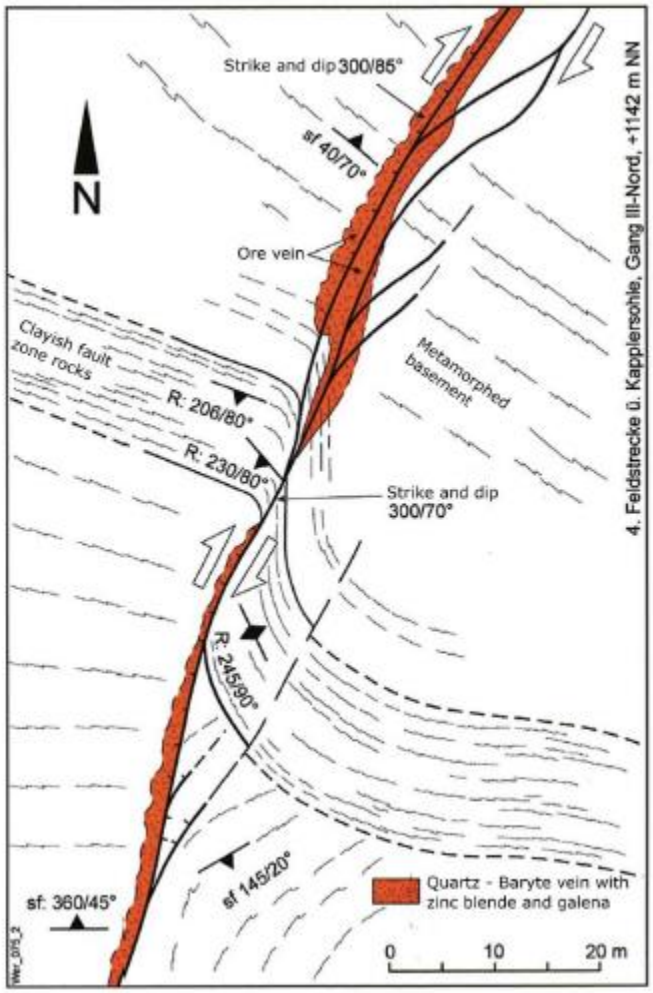

Figure 39: Scheme of the extinction of the mineral vein when encountering the highly strained shear zone (Werner, 2002)

The different geological structures were visited by ISP students during the period May 9th to 13th under guidance of mine owners (Figure 40 and Figure 41).

Figure 40: ISP students and accompanying staff at the Teufelsgrund mine entrance

Figure 41: Geological overview presentation to ISP students within the Schauinsland mine

References

Altherr, R., Holl, A., Hegner, E., Langer, C., Kreuzer, H., 2000. High-potassium, calcalkaline I-type plutonism in the european variscides: northern vosges (France) and northern schwarzwald (Germany). Lithos 50, 51–73. http://dx.doi.org/10.1016/
S0024-4937(99)00052-3.

Baillieux, P., Schill, E., Abdelfettah, Y., Dezayes, C., 2014. Possible natural fluid pathways from gravity pseudo-tomography in the geothermal fields of Northern Alsace (Upper Rhine Graben). Geotherm. Energy 2. http://dx.doi.org/10.1186/s40517-014-0016-y.
Bergerat, F., 1985. Déformations cassantes et champs de contrainte tertiaires dans la plate-forme européenne (Habilitation à Diriger la Recherche). Université Pierre et Marie Curie-Paris VI, France.

Choi, J.-H., Edwards, P., Ko, K., Kim, Y.-S., 2016. Definition and classification of fault damage zones: A review and a new methodological approach. Earth-Science Reviews 152, 70–87. https://doi.org/10.1016/j.earscirev.2015.11.006

Dèzes, P., Schmid, S.M., Ziegler, P.A., 2004. Evolution of the European Cenozoic Rift System: interaction of the Alpine and Pyrenean orogens with their foreland lithosphere. Tectonophysics 389, 1–33. http://dx.doi.org/10.1016/j.tecto.2004.06.011.
Doebl, F., 1967. The tertiary and pleistocene sediments of the Northern and Central part of the upper Rhinegraben. Mémoires du Service de la carte géologique d'Alsace et de Lorraine. pp. 48–54.
Edel, J.-B., Schulmann, K., 2009. Geophysical constraints and model of the Saxothuringian and Rhenohercynian subductions −magmatic arc system in NE France and SW Germany. Bull. Soc. Geol. Fr. 180, 545–558. http://dx.doi.org/10.2113/gssgfbull.180.6.545.
Edel, J.-B., Schulmann, K., Rotstein, Y., 2007. The Variscan tectonic inheritance of the Upper Rhine Graben: evidence of reactivations in the Lias, Late Eocene–Oligocene up to the recent. Int. J. Earth Sci. 96, 305–325. http://dx.doi.org/10.1007/s00531-006-0092-8.
Edel, J.B., Weber, K., 1995. Cadomian terranes, wrench faulting and thrusting in the central Europe Variscides: geophysical and geological evidence. Geol. Rundsch. 84, 412–432. http://dx.doi.org/10.1007/BF00260450.
Eisbacher, G.H., Fielitz, W., 2010. Karlsruhe und seine Region. Nordschwarzwald, Kraichgau, Neckartal, südlicher Odenwald, Oberrhein-Graben, Pfälzerwald und westliche Schwäbische Alb. Borntraeger Science Publishers, Stuttgart, Germany.
Fuchs, K., Bonjer, K., Gajewski, D., Lüschen, E., Prodehl, C., Sandmeier, K., Wenzel, F., Wilhelm, H., 1987. Crustal evolution of the Rhinegraben area. 1. Exploring the lower crust in the Rhinegraben rift by unified geophysical experiments. Tectonophysics 141, 261–275.
Genevois, R., Prestininzi, A., 1979. Time-Dependent Behaviour Of Granitic Rocks Related To Their Alteration Grade. Presented at the 4th ISRM Congress, OnePetro.
GeORG, 2012. Geoportail of EU-Project GeORG – INTERREG IV Upper Rhine. [WWW Document], URL http://www.geopotenziale.org (Accessed 14 April 2016).
Hafeznia, Y., Bourlange, S., Ohnenstetter, M., Flück, P., 2015. Post-meeting fieldtrip SGA 2015 meeting in Nancy: Sainte-Marie-aux-Mines Gabe Gottes Mine.
Illies, H.J., Greiner, G., 1979. Holocene movements and state of stress in the rhinegraben rift system. Tectonophys. Recent Crustal Mov. 52, 349–359. http://dx.doi.org/10.1016/0040-1951(79)90245-2.
Illies, H.J., 1972. The Rhine graben rift system-plate tectonics and transform faulting. Geophys. Surv. 1, 27–60. http://dx.doi.org/10.1007/bf01449550.
Illies, H.J., 1965. Bauplan und baugeschichte des oberrheingrabens. Oberrheinische Geol. Abh. 14, 1–54.
Lagarde, J.L., Capdevila, R., Fourcade, S., 1992. Granites et collision continentale; l'exemple des granitoides carbonifères dans la chaine hercynienne ouest-européenne. Bull. Soc. Geol. Fr. 163, 597–610.

Ledésert, B.A., Hébert, R.L., 2020. How Can Deep Geothermal Projects Provide Information on the Temperature Distribution in the Upper Rhine Graben? The Example of the Soultz-Sous-Forêts Enhanced Geothermal System. Geosciences 10, 459. https://doi.org/10.3390/geosciences10110459
Rotstein, Y., Edel, J.-B., Gabriel, G., Boulanger, D., Schaming, M., Munschy, M., 2006. Insight into the structure of the Upper Rhine Graben and its basement from a new compilation of Bouguer Gravity. Tectonophysics 425, 55–70. https://doi.org/10.1016/j.tecto.2006.07.002
Schumacher, M.E., 2002. Upper Rhine Graben: role of preexisting structures during rift evolution. Tectonics 21http://dx.doi.org/10.1029/2001tc900022. 6–1 to 6–17.
Stipp, M., Kunze, K., 2008. Dynamic recrystallization near the brittle-plastic transition in naturally and experimentally deformed quartz aggregates. Tectonophysics 448, 77–97. https://doi.org/10.1016/j.tecto.2007.11.041
Vidal, J., Genter, A. Overview of naturally permeable fractured reservoirs in the central and southern Upper Rhine Graben: Insights from geothermal wells, Geothermics, Volume 74, 2018, Pages 57-73, ISSN 0375-6505, https://doi.org/10.1016/j.geothermics.2018.02.003.
Villemin, T., Bergerat, F., 1987. L'évolution structurale du Fosse rhénan au cours du Cénozoïque: un bilan de la déformation et des effets thermiques de l'extension. Bulletin de la Société Géologique de France 8, 245–255.
Werner, W., 2004. Lagerstätten und Bergbau im Schwarzwald: ein Führer unter besonderer Berücksichtigung der für die Öffentlichkeit zugänglichen Bergwerke. Landesamt für Geologie, Rohstoffe und Bergbau Baden-Württemberg.
Werner, W., 2002. Die Erzlagerstätte Schauinsland bei Freiburg im Breisgau: Bergbau, Geologie, Hydrogeologie, Mineralogie, Geochemie, Tektonik und Lagerstättenentstehung, Aedificatio-Verlag. ed.
Wittenbrink, J., 1999. Diplomkartierung (Teil A) Petrographische und tektonische Kartierung des Zentralschwarzwälder Gneiskomplexes im Bereich der Blei – Zink – Lagerstätte Schauinsland bei Freiburg i. Br./Schwarzwald.
Ziegler, P.A., 1990. Geological Atlas of Western and Central Europe, 2nd edition. Shell International Petroleum Mij B V, London, Great Britain.

3.3 Volcanic areas

Geothermal utilization in volcanic provinces is of great interest regarding 1) the number of areas exploitable worldwide and 2) the vast amounts of energy that can potentially be gained from a single hot to superhot reservoirs.

Numerous challenges come into play, both in terms of reservoir prospection plus exploitation and technical characteristics from borehole casing to surface installations.

Geothermal energy production in Iceland has been pionnering due to its exceptional geological setting. The country is considered as a natural laboratory for studying the effects of fluid percolation in fractured oceanic crust at high temperature. Outcrop quality and active tectonics plus volcanism makes Iceland a great place for teaching geothermal sciences in the field of high enthalpy conditions.

Iceland is characterized by broad active rift zones and intense volcanism. Today, the ridge consists of four segments, the Reykjanes Volcanic Zone (RVZ), the Western Volcanic Zone (WVZ), the Eastern Volcanic Zone (EVZ) and the Northern Volcanic Zone (NVZ) (Figure 42). According to literature the Hengill area mentioned in section 2.2.3 is a intersection of the Reykjanes Volcanic Zone and Western Volcanic Zone with Iceland Seismic Zone (Li, 2019).

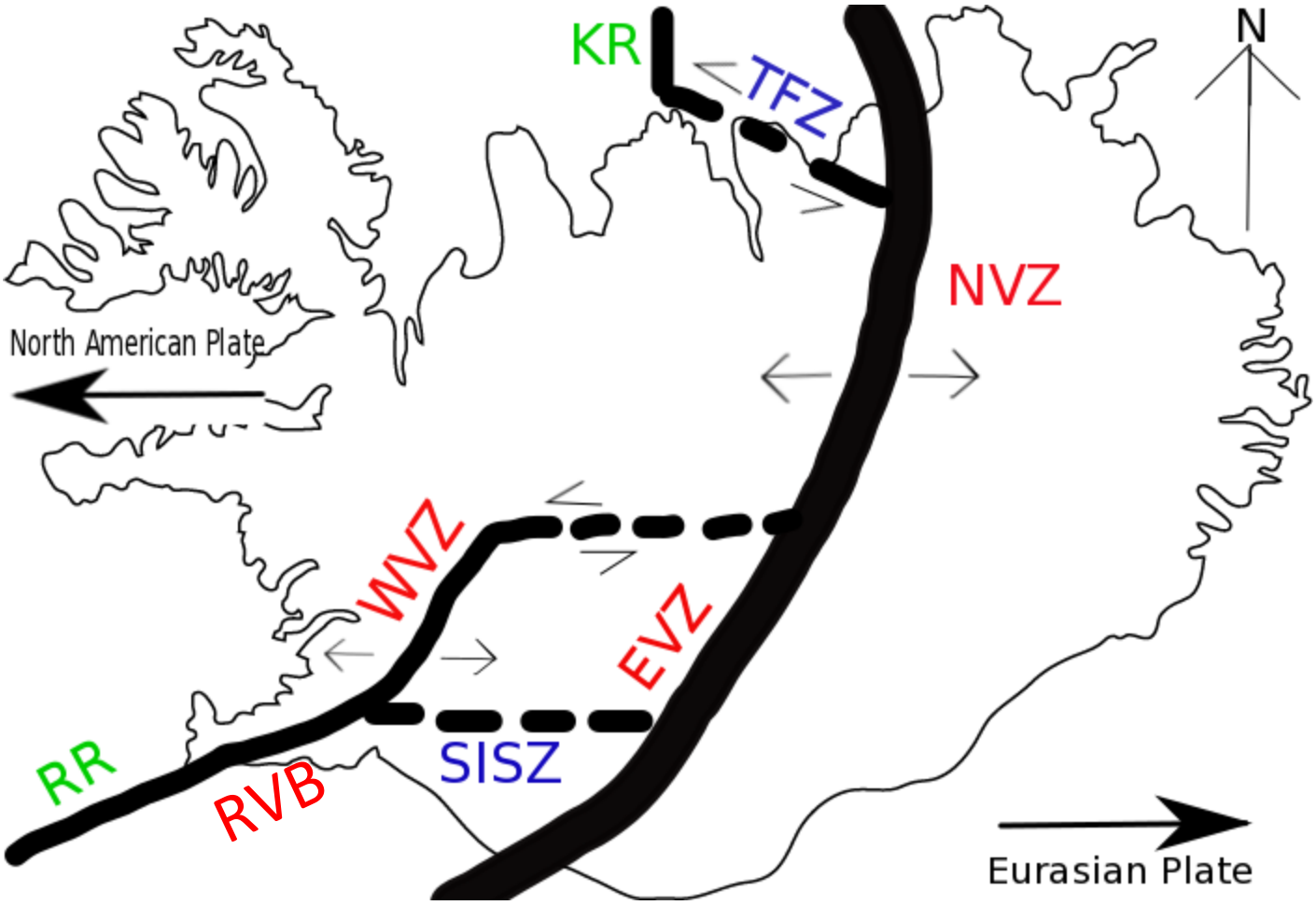

Figure 42. Main Volcanic zones in Iceland. Reykjanes Volcanic Belt (RVB), the West Volcanic Zone (WVZ), the Mid-Iceland Belt (MIB), the East Volcanic Zone (EVZ) and the North Volcanic Zone (NVZ). Two transform zones are connecting these volcano-tectonic zones: the South Iceland Seismic Zone (SISZ) in the south of Iceland and the Tjörnes transform Fault Zone (TFZ) in the north. Outside of the main island are the Reykjanes Ridge (RR), as part of the Mid-Atlantic Ridge to the southwest and the Kolbeinsey Ridge (KR) to the north.

Figure 43. ISP field excursion in Iceland

3.3.1 Reykjanes

The Reykjanes Peninsula (Figure 44) is where the mid-Atlantic ridge 'comes ashore' and hence we can see the structure of the rift and expression of the geothermal systems (both seawater and meteoric).

The mid-ocean ridge separating the North American and Eurasian runs almost E-W through the Reykjanes Peninsula, and the ridge is a seismically active strike-slip zone. In contrast, the volcanic activity has been aligned NE-SW, and forms an en-echelon series of volcanic systems with swarms of normal (extensional) faults and linear eruptive vents. The geothermal systems occur at the intersection of the volcanic systems and the seismic zone. 3 sites on the Reykjanes Peninsula were visited:

a. Seltún geothermal area
b. Fagradalshraun 2021 volcanic eruption site
c. Reykjanes geothermal area

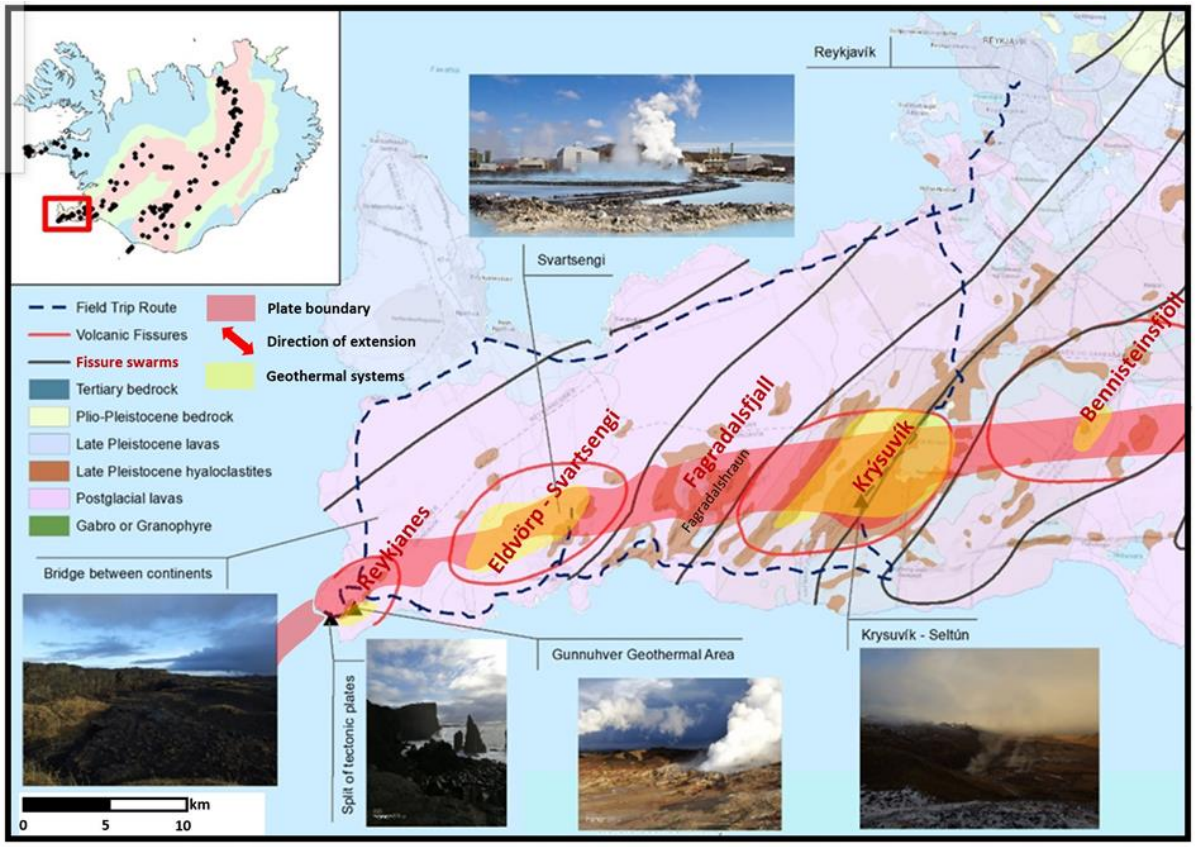

Figure 44. The main tectonic structures of the Reykjanes Peninsula. The volcanic systems are in pink, the seismic zone (the plate boundary) is in red and the geothermal systems are shown in yellow. The offshore trace of the plate boundary is in black. Modified from Hersir et al (2020).

.

3.3.1.1 Seltún

This is part of the surface expression of the Krýsuvík Geothermal system (Figure 45 and Figure 46). Seltún has steam-dominated geothermal activity, with acidic fluid (condensed steam dissolved in groundwater) and alteration of rocks to clays, resulting in mud pools and steaming ground, with near-surface (0 to 5 cm depth) temperatures of 100°C. Three deep wells and numerous shallow wells have been drilled into the Krýsuvík subsurface, although none of these are used for energy production. Temperatures in the deep wells have been measured at >300°C, although no power station has been built to utilize this system. This short visit is an introduction to the heat, power, risks and intrinsic natural uniqueness of high temperature geothermal systems.

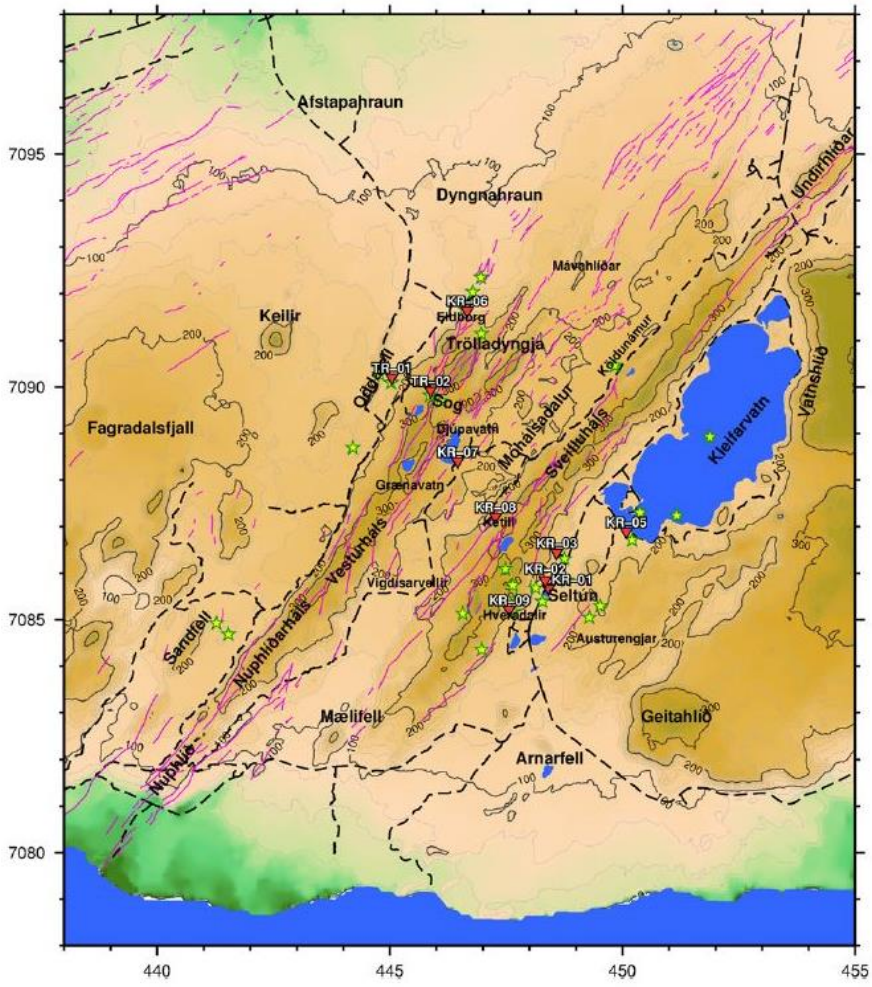

Figure 45. An overview of Krysuvik. Fumaroles, fractures and faults are according to a recent geological mapping by Saemundsson et al. (2016).Wells deeper than 300mandwell KR-01 andwell KR-03 are denoted by red filled triangles, fumaroles by green/yellowstars and fractures and faults bymagenta lines. Blue colour denotes the ocean and lakes. Modified from Hersir et al (2020).

Figure 46. Activity at Seltún, showing acidic mud pools and hydrothermally altered rock, with a carapace of less intensely-altered subglacial basaltic deposits. Photo J. Newson.

3.3.1.2 Fagradalshraun

From a geothermal point of view, the very recently formed rocks are similar to those at the Fagradalsfjall eruption form a significant volume of the geothermal reservoirs in Iceland. A close look at the physical properties of the reservoir rock gives a good understanding of how fluids might flow in the subsurface.

The Fragradalsfjall volcano eruption began on March 19th 2021, and ceased on September 18th 2021. The eruption site was visited by ISP students and accompanying staff on June 20th 2022 (Figure 47). There were 10's of 1000´s of seismic events leading up to the eruption at Fagradalsfjall, and >4000 tremors just in the 3 weeks before the eruption, which began as a fissure ~700 m long. The magma was 'primitive', meaning that it comes from the mantle, below the crust. The depth of the magma was thought to be about 17 to 20 km.

The lava flowed from the vents at 5 to 16 m^3/second, and covers a total area of 4.8 km. The volume of lava is ~ 151 M m^3. And the depth is >100 m.

As the eruption progressed, one vent became dominant, which developed a lava geyser, erupting around 8 times/hr, to a maximum height of 400 m.

Figure 47. ISP students at Fagradalshraun. This is only part of the ISP Iceland class; the others walked further to investigate the lava textures and how they might be analogues for subsurface permeability in a volcanic-hosted reservoir. Photo J. Newson.

3.3.1.3 Reykjanes

The Reykjanes geothermal system has a 100 MW geothermal power station that utilizes the dominantly seawater reservoir. The surface expression of the system is extensive, and the wellheads and surface installations (flash plant and turbine hall) are visible from the lookout. Pressure drawdown in the reservoir has caused boiling and an increased steam flow to the surface, resulting in an increased area of hot ground.

In 2016 drilling commenced on a special well, the second well in the Iceland Deep Drilling Program (IDDP2). This was designed to access the supercritical conditions in the much deeper zone of the geothermal system than is usually accessed by geothermal wells (which are generally less than 3500 m deep. In addition, there was particular interest in this well because it was drilled into the mid-ocean ridge, because there is much to be understood about this geologic, geochemical and geothermal environment. The well was drilled to 4659 m and has been warming since then. Unfortunately casing corrosion damage while warming due to the aggressive nature of the fluids from these deep conditions, has limited the amount of available data.

3.3.2 Þjórsárdalur (Gjáin and Háifoss)

Gjáin and Háifoss are waterfalls in the Þjórsá river valley (Þjórsádalur). These flow over outcrops of various basalt flows which exhibit well-developed cooling fractures (Figure 48).

At Gjáin there are around 0.92 million years of activity represented by the basalt flows. The stratigraphic sequence is as follows: youngest flow is the Búrfellshraun (thi), sourced from the Veiðivötn Volcanic fissure swarm to the east, and is dated at ~3200 years bp (Halldorsson et al, 2008). However, this is topographically lower than many of the older lavas, due to having filled the valleys. The surface lava at Gjáin is the Sandafell olivine tholeiite (sao) (087 to 0.92 million years bp) and which is underlain by the Sámsstaðamúli porphyritic basalt (smd) (>0.92 million years bp). Undefined sediments (sd) may occur between the lavas. The sequence is underlain by the Reykholt hyaloclastite (rem).

At Háifoss, which is topographically higher than Gjáin, the surface rock is the Stangarfjall tholeiite (stþ), underlain by a similar sequence to the Gjáin outcrop, absent the Sandafell olivine tholeiite, but including the Reykholt tholeiite.

This sequence of lava flows shows very clearly the nature of fracture permeability in a laterally extensive flows should they occur in a geothermal reservoir.

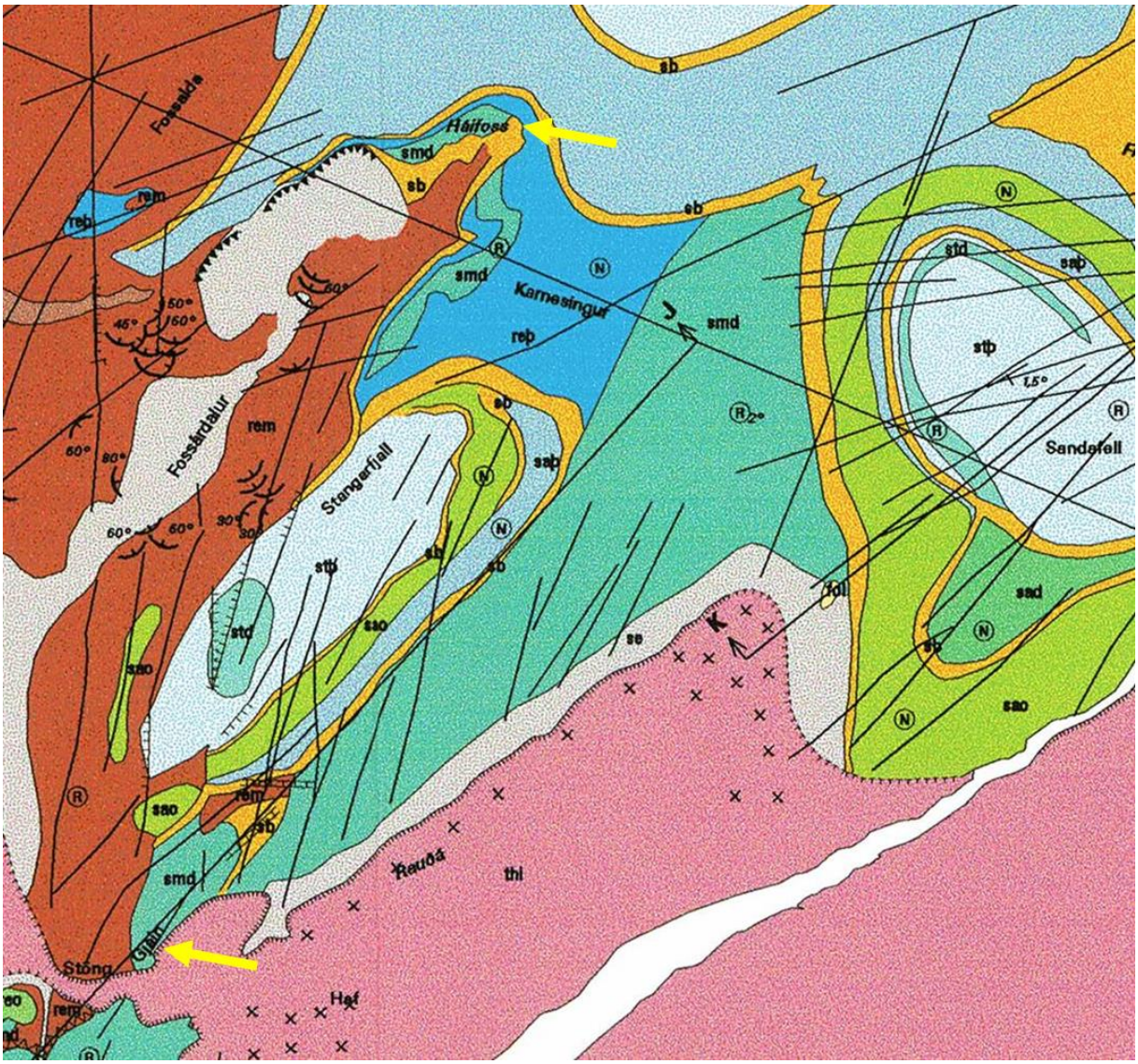

Figure 48. Geological map of the Gjáin-Háifoss area from https://orkustofnun.is/vefsjarmyndir/1028.jpg . The yellow arrows point to the locations of Háifoss and Gjáin. Symbols for the lithologies are: thi=Búrfellshraun; stþ=Stangarfjall tholeiite; sao=Sandafell olivine tholeiite; smd=Sámsstaðamúli porphyritic basalt; rep=Reykholt tholeiite; rem=Reykholt hyaloclastite.

3.3.3 Landmannalaugar and the Torfajökull Volcano

Landmannalaugar area is within the Torfajökull Central Volcano, the largest silicic volcanic complex in Iceland (Figure 49 and Figure 50). There have been mixed-magma eruptions in the area related to crustal rifting, whereby tholeiitic magma is thought to have been injected into the rhyolite magma chamber.

Several mixed rhyolite-basaltic lava flows occur in the Torfajökull area; the most recent are from the Veidivötn fissure swarm, which terminates on the northern margin of the Torfajökull volcano. These include the Dómadalshraun flow and the more recent Námshraun (sometimes referred to as Sudurnámshraun) and Laugahraun flows (Wilson et al 2007). The hot stream at Landmannalaugar flows from beneath the northeastern margin of the Laugarhraun flow, which in this vicinity comprises chaotic blocks of obsidian. The southeastern margin of Laugarhraun is defined, across the Grænágil Gorge, by the subglacial Bláhnukur rhyolite (de Vet and Cammeraat, 2012).

The geothermal waters at Torfajökull are either steam-heated groundwater or mixed, boiled reservoir water. The steam–heated waters are either sulfate-rich or bicarbonate –rich waters. The reservoir waters are chloride water with concentrations between ~50 to 600 ppm (Björke et al, 2015).

There are no energy developments utilizing the geothermal system related to the Torfajökull volcano. However, the Landmannalaugar area is very beautiful, and the most popular tourist destination in the Icelandic Highlands. The total number of visitors to Landmannalaugar reached 120,000 annually by 2009 (Saeþorsdottir, 2013). Thus the economic value of the system is in its intrinsic beauty, and tourist value of the geothermal and volcanic resource.

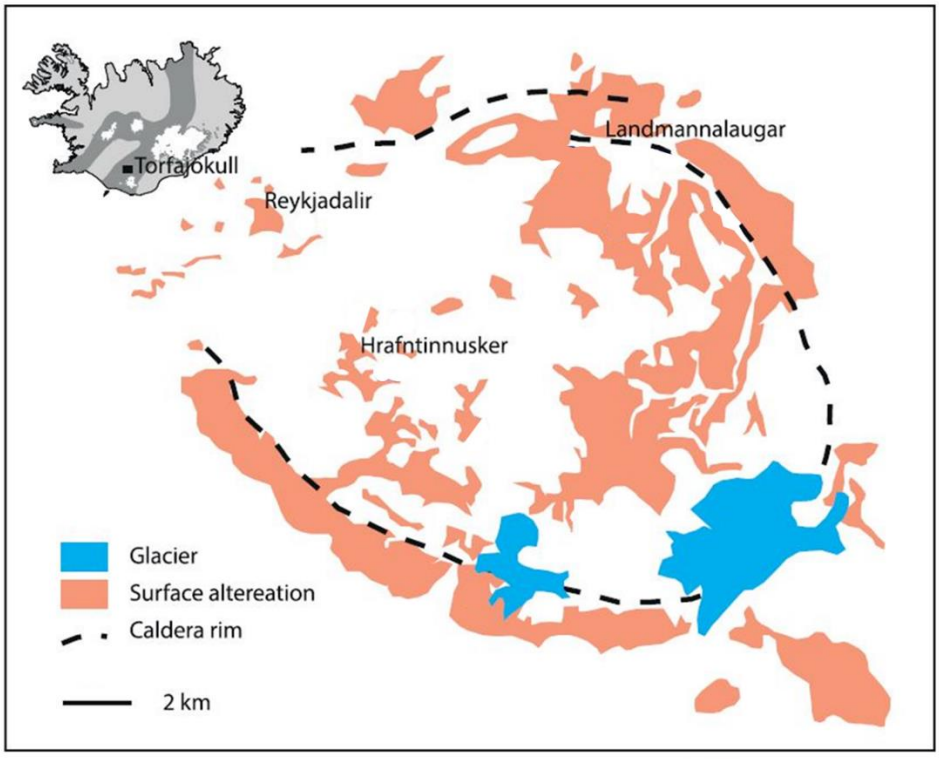

Figure 49. The Torfajökull Volcanic area, showing Landmannalaugar on the northern edge of the caldera (adapted from Björke et al, 2015).

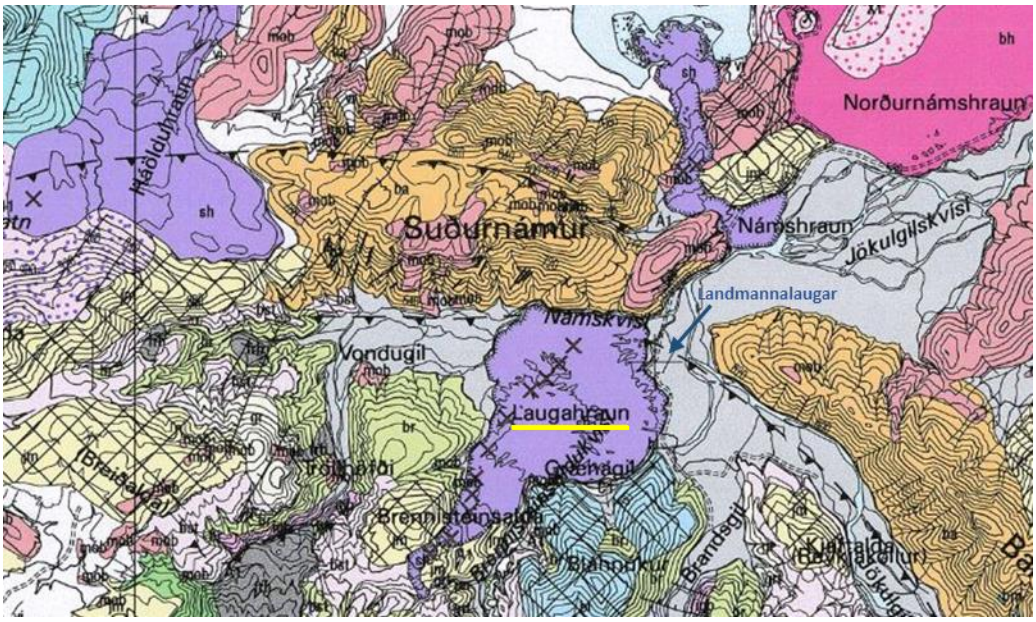

Figure 50. Geologic map of the northern margin of the Torfajökull Volcano, showing the Laugahraun (underlined in yellow), and the Landmannalaugar area to the northeast of the lava flow (from https://orkustofnun.is/vefsjarmyndir/873.jpg).

The area was visited by ISP students and accompanying staff on June 23rd (Figure 51).

Figure 51. Students on the surface of the Laugarhraun flow, near steam activity (background middle left). Photo J. Newson.

References

J.K. Björke, A.Stefánsson, S. Arnórsson (2015). Surface water chemistry at Torfajökull, Iceland—Quantification of boiling, mixing, oxidation and water–rock interaction and reconstruction of reservoir fluid composition. Geothermics 58 (2015) 75–86.

S. J. de Vet, E. L.H. Cammeraat (2012). Aeolian contributions to the development of hillslopes and scree sediments in Grænagil, Torfajökull, Iceland. Geomorphology 175–176 p74–85.

S. A. Halldorsson, N. Oskarsson, K. Gronvold, G. Sigurdsson, G. Sverrisdottir, S. Steinthorsson (2008). Isotopic-heterogeneity of the Thjorsa lava—Implications for mantle sources and crustal processes within the Eastern Rift Zone, Iceland. Chemical Geology 255 p305–316.

G. Hersir, K. Árnasona, A. M. Vilhjálmsson, K. Saemundsson, Þ. Ágústsdóttir, G. Ó. Friðleifsson (2020). Krýsuvík high temperature geothermal area in SW Iceland: Geological setting and 3D inversion of magnetotelluric (MT) resistivity data. Journal of Volcanology and Geothermal Research 391.

Li, K. L. (2019). Seismicity of the Hengill Area, SW Iceland: Details Revealed by Catalog Relocation and Collapsing. Journal of Volcanology and Geothermal Research, 15-26.

A. D. Sæþórsdóttir (2013). Managing popularity: Changes in tourist attitudes in a wilderness destination. Tourism Management Perspectives 7 p47–58.

L. Wilson, S.A. Fagents, L. E. Robshaw, E. D. Scott (2007). Vent geometry and eruption conditions of the mixed rhyolite–basalt Námshraun lava flow, Iceland. Journal of Volcanology and Geothermal Research 164 p127–141.

3.4 Orogen foreland domain

The southern part of the subalpine chain (Figure 52) is a geologically complex area, superimposing episodes of compressive deformation and forming sedimentary basins related to the Alpine orogenic prism. The objective here is to use the Southern Subalpine Folded Range as an example to analyze the reservoir capacity of the formations in this area, more precisely, those located within the foreland basin. The study of sedimentary facies can be linked to the geometry of local tectonic structures, whose location and orientation testify to the evolution of sedimentation in the South Alpine foreland basins. This work (Menut et al. 2022) is based on field observations, cross-sections, and stratigraphic logs, and on scientific publications allowing a better understanding of certain specificities, whether on stratigraphy, reservoir capacities or local tectonics.

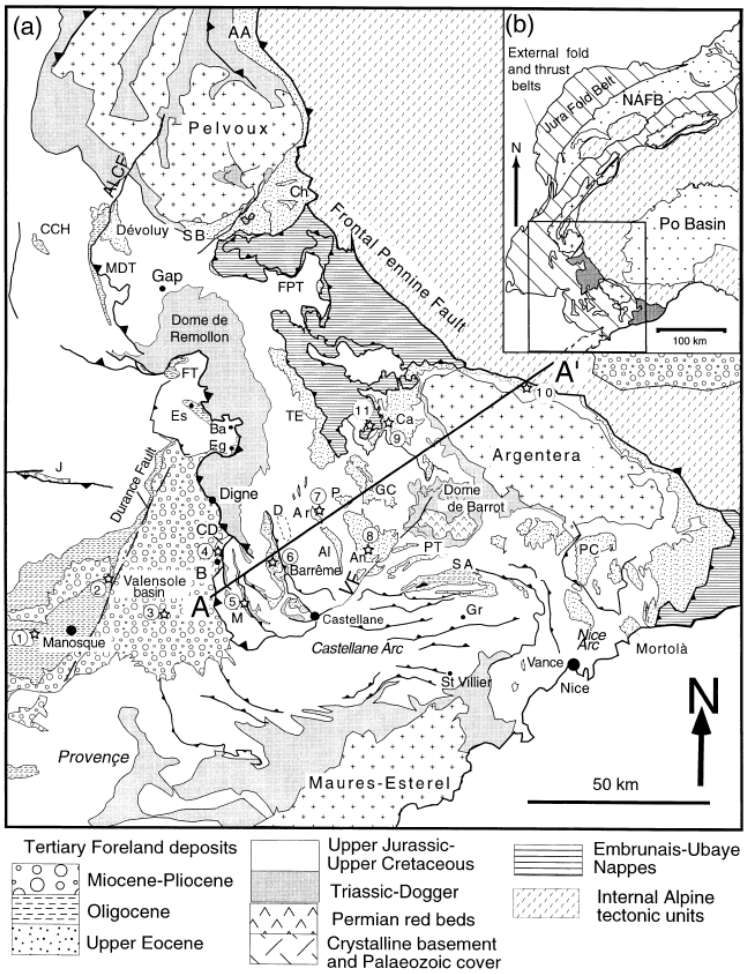

Figure 52. geological map from Ford et al. 2002, representing the main domains of southern sub alpine foreland basins.

Foreland basins are formed in a compressional context. They originate from the flexure of the overlapped lithosphere following the application of a load on it. They are located at the front of orogenic prisms and can be discriminated into two types: the pro-wedge and the retro-wedge. The first is formed on the subducted plate, the one with the maximum subsidence and is called a foreland flexural basin. The second is formed on the overriding plate. The Alps being a double vergence chain resulting from the subduction of Europe under Apulia, the basin whose relics are mapped in the Digne-Castellane area is a foreland basin of pro-wedge type. In the southwestern part of the chain between Digne and Valensole, the orientation of these basins is generally NW-SE, in contrast to the SW-NE orientation of the Swiss Molasse basin. This particularity is explained by the fact that the Alpine chain is arched (Lickorish et al., 2002).

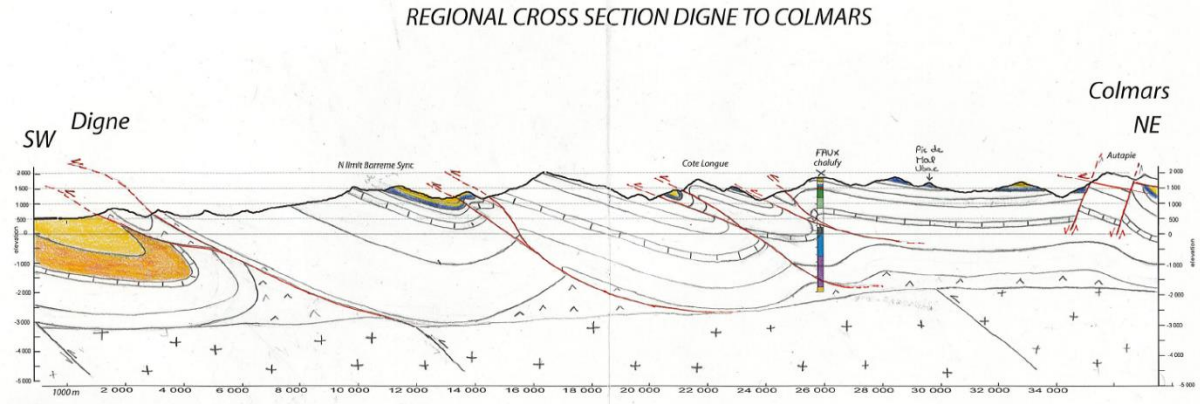

Figure 53. Regional cross-section in the southern Alps, between Digne and Colmars (Menut et al., 2022).

On the regional cross-section (Figure 53), the succession of folds by fault propagation is visible, with large thrusts anchored in the Keuper or the Terres Noires. The Tertiary deposits in the localities of Barrême and Colmars are at the heart of these two synclines. However, the unconformity of these Cenozoic sediments is also found in the Chalufy massif, and in the last basin to have functioned in this southern subalpine chain, namely the Digne-Valensole basin, whose Mio-Pliocene filling is consistent in this section. The thickness of most of the formations remains constant, except for the Upper Cretaceous whose thickness increases from East to West before disappearing in the West by erosion. The Lias is very thick in the syncline of Barrême, then thins under La Valette. We propose the presence of a tilted block of the European passive margin, in agreement with the section of Lickorish and Ford, 1998. The associated normal faults are reactivated during alpine compression and are coupled with large thrusts in the sedimentary cover.

A reservoir rock is a rock that can hold fluids for accumulation. Multiple factors control fluid flow and storage in sedimentary rocks. Matrix porosity controls storage properties at the millimeter scale, while the density and openness of fractures and faults control transfer properties at the decameter scale. The geometry of layers in the basin controls large-scale flows. For a rock to have the capacity to circulate fluids or to store them, it is necessary that it presents a high porosity and permeability. Porosity and permeability change in time and space as a result of diagenetic transformations and tectonic deformation, which occur on a million-year scale.

Three families of rocks are predominant in the area studied: sandstones, limestones and clays. Sandstones can be good reservoir rocks because they are composed of an assembly of grains of sand and therefore present an inter particular permeability. Limestones are not very porous and not very permeable when they are healthy. However, if they are altered or undergo diagenetic transformation, they can become good reservoirs. For example, the alteration can lead to the formation of fractures which gives the rock a so-called fracture permeability, and a common diagenetic phenomenon is dolomitization which greatly increases the permeability of the limestone (now a dolomite). Clays are very low permeability and porous and are therefore poor reservoirs. Even very thin layers can disrupt fluid flow in the surrounding rocks.

Several formations such as the Annot or Sénez sandstones, the nummulitic limestones or the tithonic limestones seem, a priori, to present exciting characteristics in terms of reservoirs. For the limestones, it remains to be verified if a fracturing or a diagenetic transformation could have changed the characteristics of these rocks, which could be conducive to fluid circulation.

Regarding geothermal energy, the reservoir can be open. A zone can be exploited under the conditions that the thermal gradient is sufficient, that the water circulates at depth and can remain there for the time necessary for its heating.

All these structures are favorable to traps and can be observed in the studied area. In relation to the structural geology part, the presence of rocks with petrological reservoir characteristics and elements constituting the traps leads us to think that the area could present reservoirs or analogs for geothermal exploration.

References

Ford, , Lickorish, and Kusznir, (1999), Tertiary foreland sedimentation in the Southern Subalpine Chains, SE France: a geodynamic appraisal. Basin Research, 11: 315-336.

Lickorish, W. H., Ford, M., Burgisser, J., Cobbold, P. R., 2002. Arcuate thrust systems in sandbox experiments: A comparison to the external arcs of the Western Alps. Geological Society of America Bulletin, 114(9), pp. 1089-1107.

Lickorish, W.H., Ford, M., 1998. Sequential restoration of the external Alpine Digne thrust system, SE France, constrained by kinematic data and synorogenic sediments. In: Mascle, A., Puidefàbregas, C., Luterbacher, H.P., Fernàndez, M. (Eds.), Geological Society of London Special Publication, 134. Cenozoic Foreland Basins of Western Europe, pp. 189–211.

Menut A., Didier C., Eguin, R. 2022 Exploration and reservoir investigation: case study of the southern folded ranges, Field report, Ecole Nationale Supérieure de Géologie, Nancy, France.

4 Petrophysical investigations in the laboratory

During the week May 16th to May 20th 2022, students have the opportunity to follow the complete process of petrophysical property measurements on representative facies rock samples from the different geothermal reservoirs under guidance of TU Darmstadt staff members (Figure 54 and Figure 55). This laboratory expertise is of prime importance for reservoir engineers when numerical reservoir exploitations are to be designed. Petrophysical input is mandatory for realistic flow and reservoir temperature evolution trough time models to be produced.

The hydrothermikum platform accessible at the TU Darmstadt provides to the students High-tech analytics and an interdisciplinary laboratory concept offer a broad spectrum of investigation options.

The interdisciplinary laboratory concept of the HydroThermikum offers a broad spectrum of geothermally, hydrogeologically and sediment-geologically relevant analysis options for solid and unconsolidated rocks as well as fluids. It consists of a thermophysical laboratory, permeametry and porosimetry, a thermo-triax stand, as well as geotechnical, hydrochemical and sediment geological laboratories.

The properties that can be determined in the framework of the geo3en programm in the laboratory facilities of the TU Darmstadt are:

4.1 Permeability and porosimetry

These two parameters are key properties in reservoir characterisation.

For porosity determination, the laboratory is equipped with three helium pycnometers and one powder pycnometer. One helium pycnometer can hold samples of up to two litres in volume.

The permeability determination covers an extremely wide measuring range from 50 D [Darcy] to 1µD. Since permeability is a tensor, the laboratory is able to measure the permeability of samples in three dimensions. This can be done as apparent permeability with a so-called mini-permeameter, as well as with intrinsic permeability, which is measured with enclosed samples and different pressure levels. The medium used is mainly air, but liquids can also be used. The laboratory has one mobile and two stationary devices.

4.2 Thermophysics laboratory

When determining thermal conductivity using the optical scanning method, the emitter and measuring unit is moved along the sample. The emitted light and heat radiation is focused on the surface of the sample, heating it up. Infrared temperature sensors are located at a fixed distance from the emitter and measure the temperature of the sample before and after heating. By comparing this with known standards, the thermal conductivity can be determined. The main components of the measuring device are shown in Figure 1; the figures below show the Thermal Conductivity Scanner and the mobile Lamda Measurement Centre (LMC). A full- and half-space line source measuring device (TK 04) is also available for determining the thermal conductivity on unconsolidated rocks. By means of a modified evaporation test, thermal conductivities with different degrees of saturation can be determined on unconsolidated rocks or building material samples.

By means of a calorimeter (Setaram C-80), heat capacities of solids can be determined in the temperature range of 20-300°C.

Determining these properties is essential to have a databank to modelise reservoir rock properties, and to estimate uncertainties relative to these values, depending on facies heterogeneity.

4.3 Rock mechanics laboratory

By determining the unconfined compressive strength on oriented drill cores from the outcrops or from well cores, it is possible to conclude the stress field in the rock mass and thus about the relationship between rock stress and structure (fracture system, faults) that governs permeability. The thermotriax cell can then be used to validate these conclusions under actual temperature and pressure conditions. The figure below shows a schematic drawing to distinguish between rock stress controlled permeability and microstructure controlled permeability.

4.4 Thermotriax facility

In order to represent real reservoir conditions, temperature- and pressure-dependent changes in the characteristic values must be taken into account. For this purpose, values can be calculated for water-saturated rocks under realistic pressure and temperature conditions for relevant depths. These determined characteristic values can be validated by means of a thermotriax cell. The thermotriax cell can simulate the temperature and pressure conditions prevailing in the target formation and thus offers the possibility of applying pore water pressures to rock samples from the outcrop analogues under realistic reservoir

conditions and determining their permeability. Experiments in the new triaxial test facility provide characteristic values that enable the numerical simulation of the influences of constant circulation, extraction and reinjection of fluids at different temperatures in the reservoir. The range of rock permeabilities that can be investigated extends from technically dense (up to about 1E-16 m²) to highly permeable (1E-9 m²). Turbulent unsteady flow systems are thus just as adjustable as laminar steady states. The continuously temperature-controlled (0 - 200°C) high-pressure inner cell of the Felstriaxial and permeability testing system is made of V4A steel and is resistant to a wide range of highly aggressive fluids. Various hydrothermal waters containing e.g. sulphuric acid and carbonic acid can be used. Flow-through tests are used to determine permeability and quantify hydrothermal alteration. Permeability can be determined under transient (shut-in) conditions or steady-state continuous flow conditions. For this purpose, up to 500 bar pore pressure is applied to the sample separately by the lower and upper exchange rams. The samples are loaded either statically or dynamically in the cell.

The students were assisting to experimental procedures, and this visit gave them insights how coupled parametrisation of rock properties, between thermo, mechanicaco, hydro, and chemical changes.

Figure 54. Hydrothermikum lab visit and experimentation from students to characterize multi parameters petrophysical behavior of rock samples

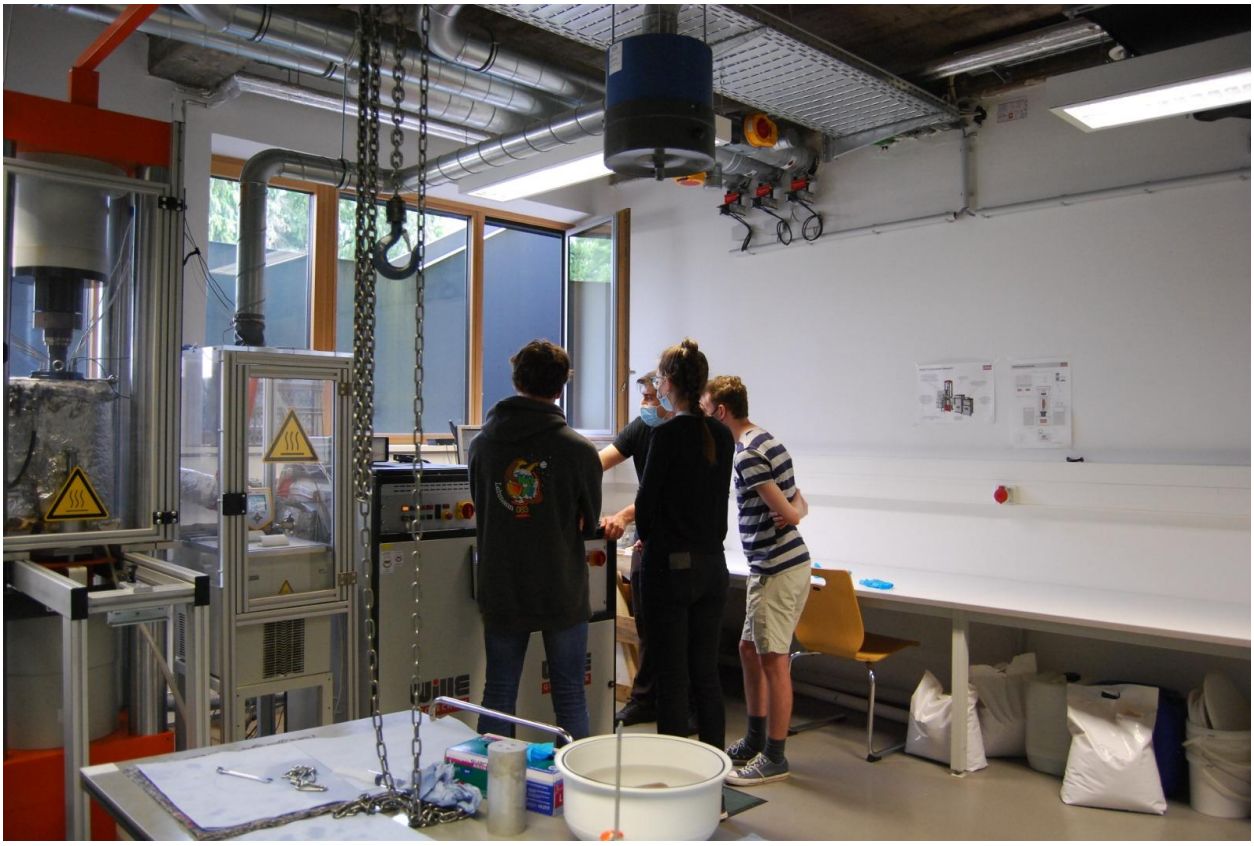

Figure 55. ISP Students performing experiments with mentoring in the Thermo-triax facility necessary for optimal permeabilities for geothermal reservoir rocks samples.

5 Turbine engineering

Electricity production by means of geothermal or other energy sources require knowledge in the field of turbine engineering as these are major components within flow diagrams. In the following turbine types are briefly described and some units visited in the framework of the ISP programme are presented.

5.1 Turbine types

Turbines are machines that drive synchronous/asynchronous generators that produce electricity based on mechanical-electromagnetic conversion. The electrical power of the generator is equal to the power of the turbine reduced by the losses in the generator. Like the generator, the turbine has also losses, but the efficiencies of both machines are high, over 90%. The type of turbine depends on the fluid that drives it, so we have steam turbines, gas turbines, hydro turbines and wind turbines. As far as generators are concerned, synchronous generators are most often used today, while asynchronous generators are used for lower power, e.g. in some types of wind turbines.

5.2 Steam turbines

Geothermal power plants primarily use steam turbines. Dry steam power plants directly use geothermal saturated steam which is superheated by decreasing the pressure before entering the turbine. The flash steam power plants use saturated liquid that is pumped out of the geothermal reservoir (Figure 56). In order to produce steam from liquid water, water is first expanded through an expansion valve resulting in two-phase flow. The mixture of liquid and vapor is separated afterwards in the separator after which steam is directed to the steam turbine to generate electricity while the remaining liquid is reinjected to a reinjection well.

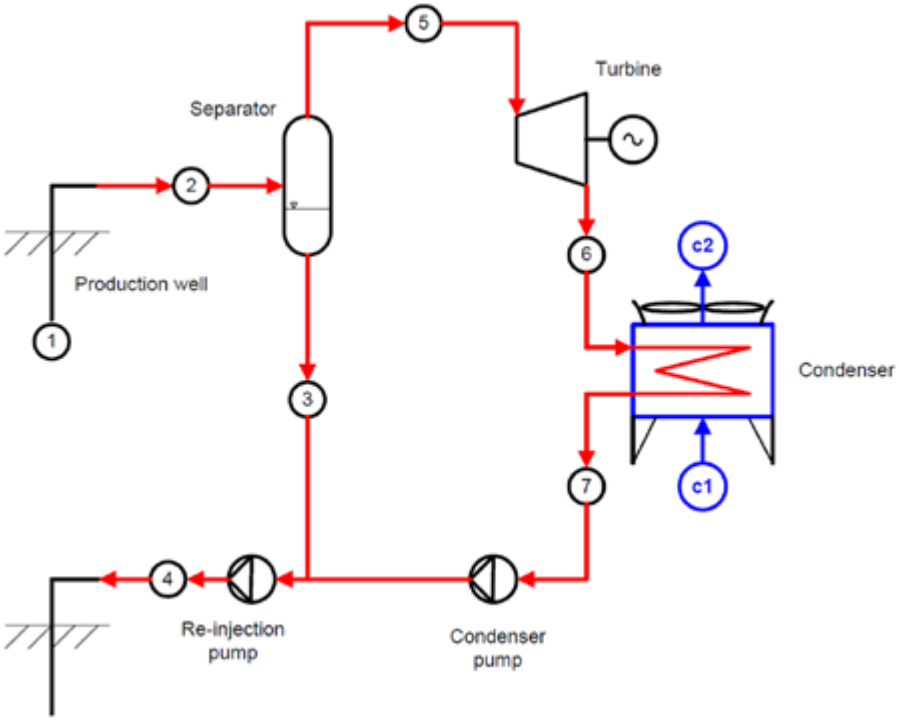

Figure 56. Flow diagram of a flash steam geothermal power plant (El Haj Assad et al., 2017)

There are two types of steam turbines: impulse and reaction turbines. The impulse turbines work at constant steam pressure across the rotor blades. The conversion of enthalpy into kinetic energy occurs in stator nozzles where a high vapour velocity is achieved. In the reaction turbines there is a pressure drop both in stationary and rotor blades (both pressure and velocity change as the steam flows through the rotor blades). Decrease in velocity/pressure means that energy from steam is extracted to apply the torque on the shaft which connects the turbine and electrical generator. That mechanical energy is converted in electricity in the generator. The blades of these turbines differ in design: the impulse blades are more symmetrical in shape around the radial axis, while the reaction blades are a bit longer and asymmetrical. Usually, the impulse blades are used for higher steam pressures, and the reaction blades for lower pressures. As the steam pressure decreases, the volume of steam increases which means that reaction blades have higher diameter than impulse blades.

The steam turbines consist of multiple stages (combination of stator nozzles/fixed blades and rotor blades in series on the same shaft), rather than a single stage (Figure 57). This construction is called compounding and is used to reduce the rotor speed. There are three types of compounding: velocity, pressure and pressure-velocity compounding. The velocity compounding is used for impulse turbines. The high pressure/velocity steam exits the nozzles and is directed in the first stage of moving blades. After that it is exhausted on the next ring of fixed blades which are used to redirect the steam leaving from the first ring of moving blades to the second ring of moving blades. There is no change in the velocity of the steam as it passes through the fixed blades. The velocity decreases through the moving blades. The pressure remains constant both in the fixed and moving blades. Pressure compounding could be applied to both impulse and reaction turbines. The velocity profile is similar in both types of turbines. Velocity increases in nozzles/fixed blades and decreases through the moving blades. On the other hand, pressure decreases continuously through fixed and moving blades in reaction turbines, while in impulse turbines it decreases in nozzles, but remains constant through moving blades. The pressure velocity compounding is used for impulse turbines and is similar to velocity compounding. The only difference is that turbine stages are divided into sets. Each set has a velocity compounding and between them are nozzles used to decrease the total pressure and increase the velocity.

Figure 57. Multistage steam turbine (Chisley and Prescott, 2013)

Steam turbines have two types of losses: mechanical and thermodynamic losses. Mechanical losses occur in components such as bearings, seals, etc. Thermodynamic losses are related to the process of steam expansion in the turbine. Ideally, the entropy in the turbine is unchanged, while in the real case it increases, which means that less enthalpy is converted into kinetic energy. Steam turbine efficiency is a measure of how efficiently the turbine extracts power from the steam and converts it into kinetic energy. Multistage steam turbines have thermodynamic (isentropic) efficiencies that vary from 65% for turbines with power less than 1 MW to over 90% for large turbines with power greater than 100 MW. Single stage steam turbines have low efficiencies (< 50%).

During the ISP students visited thermal power plant EL-TO Zagreb that produces both electrical and heating power (Figure 58). Electric power output is 50 MW and heat power 280 MW. For electricity production it uses steam and gas turbines. Energy sources are fuel oil and natural gas.

Figure 58. ISP students at the EL-TO Zagreb thermal power plan (Croatia)

5.3 Turbines for organic fluids

The arrangement of geothermal power plants with binary cycle (Figure 59) is a bit different. The binary cycle is used when the temperature of geothermal water is too low to be able to use the flash steam process, i.e., the efficiency of such a cycle would be low if implemented. In this case, an organic medium with a low evaporation temperature and, more importantly, with a low latent heat of vaporization is used in the secondary circuit. Hence the name of this cycle – organic Rankine cycle (ORC). Temperature-entropy diagram for some organic candidates is shown in Figure 60. In a specially designed heat exchanger, heat is transferred from geothermal water to an organic medium that is preheated, evaporated and, if necessary, superheated in the heat exchanger. An additional advantage of this fluid is that after expansion in the

turbine, it ends up in a superheated area, which increases the turbine thermodynamic efficiency and prevents possible damage of turbine blades by liquid droplets. These turbines are, therefore, similar to steam turbines, but are adapted to the organic medium and its thermodynamic properties.

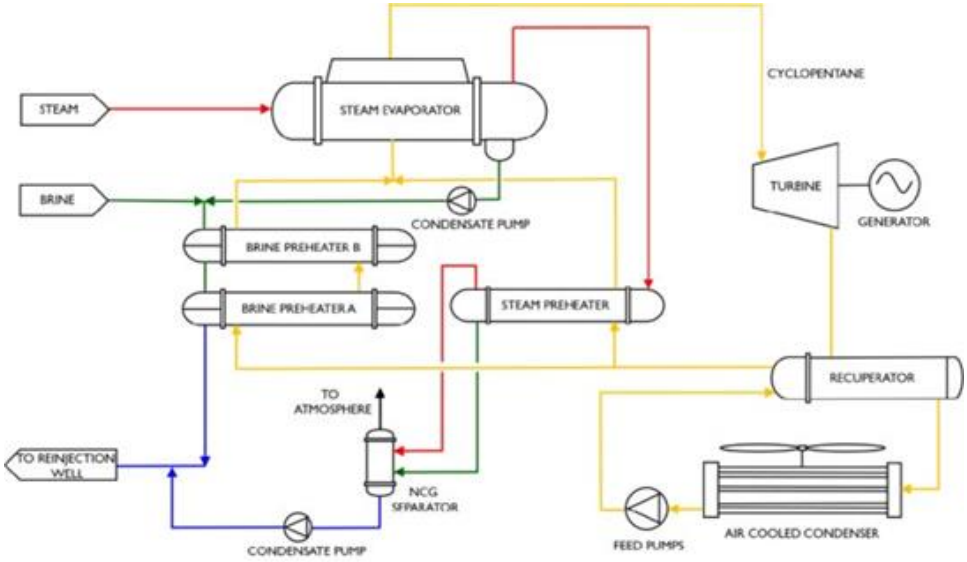

Figure 59. Flow diagram of geothermal power plant with binary cycle (Franco et al., 2017)

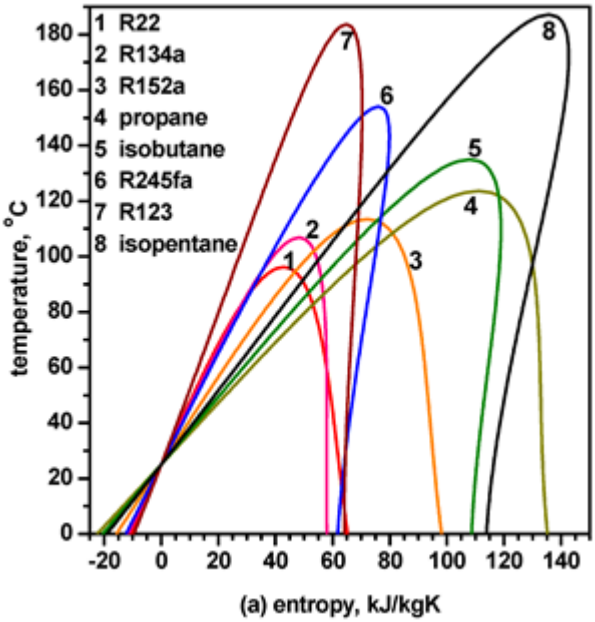

Figure 60. Temperature-entropy diagrams of organic fluids (Lee and Kim, 2015)

The standard axial steam turbines are not applicable for organic fluid with low enthalpy and low-quality heat source of geothermal water. Instead, a radial outflow turbine (ROT) is used with higher efficiency than axial turbines. The ROT is composed of multiple stages of radially positioned blades (Figure 61). Compared to axial turbines, the radial outflow turbines can operate at larger flows and enthalpy drops. They have a high isentropic efficiency and low level of noise and vibrations.

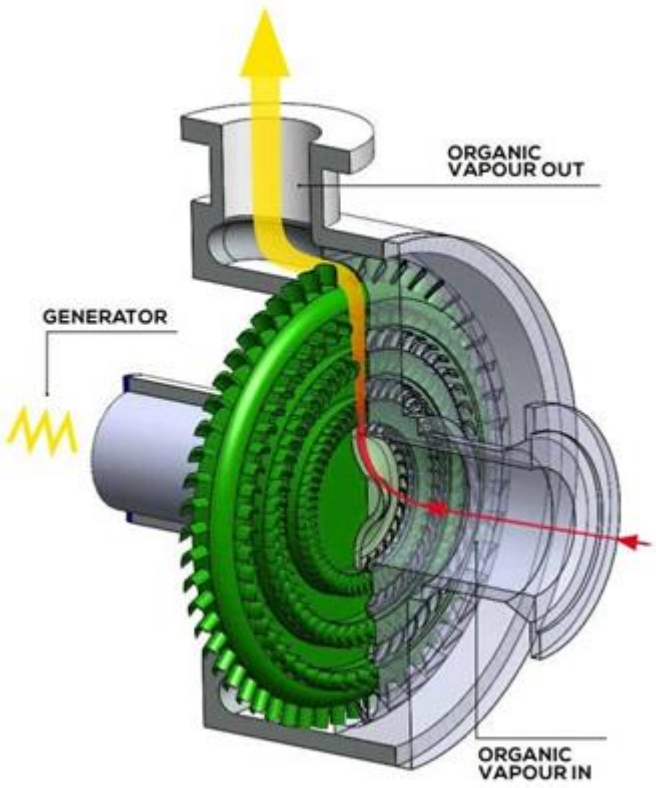

Figure 61. Radial outflow turbine used in geothermal power plant with binary cycle (Franco et al., 2017)

In Velika 1 power plant in Ciglena a turbine with 15 MW nominal power is used (Figure 62). It has five stages that allow to reach an isentropic efficiency of up to 91%. The rotating speed is 1.500 rpm (no use of reduction gear is needed).

Figure 62. Housing of a turbine used in power plant Velika 1

5.4 Water turbines

Hydro, or water turbines convert potential and kinetic energy of water into mechanical work. They are integral part of hydro power plants in which electrical energy is produced using water energy. Hydroelectric power plants use dams to create an accumulation lake and divert water from the original stream bed towards the penstock (pressure tunnel) that delivers water to turbine. There are two types of hydro power plants depending on the size of the water reservoir: the conventional hydro power plants that use large reservoirs and can store large amounts of water for longer time period, and the run-of-the-river plants with small accumulations where only water coming from upstream is available for power generation at that moment, and any oversupply passes unused. The power of hydro power plants depends on two parameters: the head (difference in height between the source and the water's outflow) and the flow rate. The flow rate depends on the flow rate of the river. The total flow of the river cannot be redirected to the turbine but part must be discharged into the original stream bed in order not to dry out (residual/ environmental minimum).

The efficiencies of modern water turbines are greater than 90%. Water turbines can be impulse or reaction turbines. Their selection depends on various parameters but, in general, for the high-head applications impulse turbines are used, and for the lower head, the reaction turbines. Today, the impulse turbine used is the Pelton turbine, or Pelton wheel. Around the rotor consisting of fixed spoon-shaped blades there are nozzles directing high-speed streams of water towards the rotor blades exerting the torque on the turbine shaft. As in all impulse turbines, the pressure in the rotor wheel is constant and equal to atmospheric pressure. The pressure across the rotor blades decreases in reaction turbines. The most common types of reaction turbines used today are Kaplan and Francis turbines. Kaplan turbines are used in low-head applications (< 50 m) where its efficiency is higher than Francis turbines which are used at medium-head

conditions. The rotor blades of Kaplan turbine can be adjusted for power and efficiency control, whereas the rotor blades are fixed in the Francis turbine. The wicket gates of both turbine types are adjustable.

Hydro power plant Varaždin on Drava river was visited during the ISP in Croatia (Figure 63). It uses two Kaplan turbines with maximum power 2×47 MW and maximum discharge 250 m^3/s per turbine. The average annual output is 450 GWh. The reservoir surface area is 3 km^2 and storage capacity 8×10^6 m^3. The length of diversion canal is: headrace canal 7.4 km, tailrace canal 7.2 km. The gross head is 20-24 m.

Figure 63. Students in front of the Kaplan turbine in hydro power plant Varaždin in Croatia

At the University of Zagreb, Faculty of electrical engineering and computing in Smart grid laboratory there is a small hydro power plant with Pelton turbine (Figure 64). The power plant consists of a 7000 l water basin underneath the lab, a Pelton turbine with nominal flow of 27 l/s, a synchronous generator (20 kVA) and the corresponding control and protection system. The water is pumped from the basin to the turbine simulating the penstock. The rated speed is 1000 rpm, voltage 380 V and rated power factor 0.5.

Figure 64. Pelton hydraulic turbine and synchronous generator at University of Zagreb

References

El Haj Assad, M., Bani-Hani, E. & Khalil, M. Performance of geothermal power plants (single, dual, and binary) to compensate for LHC-CERN power consumption: comparative study. Geotherm Energy 5, 17 (2017). https://doi.org/10.1186/s40517-017-0074-z

Eugene A. Chisley, Eric Prescott. Steam Turbine Blade Reverse Engineering, Upgrade, and Structural Design. Power (2013). https://www.powermag.com/steam-turbine-blade-reverse-engineering-upgrade-and-structural-design/

Lee, H.Y.; Kim, K.H. Energy and Exergy Analyses of a Combined Power Cycle Using the Organic Rankine Cycle and the Cold Energy of Liquefied Natural Gas. Entropy 2015, 17, 6412-6432. https://doi.org/10.3390/e17096412

António Franco, Nuno Vieira, Carlos Ponte. Geothermal developments in Pico Alto, Terceira Island, Portugal. Conference: Geothermal Resources Council Transactions, Davis, California. Volume 41. October 2017.

6 Environmental Impact Site-Visits

Renewable energy production aims at decreasing the amount of green house gases emission in the atmosphere. Geothermal energy utilization must also take into account a variety of regulations in terms of environmental impact and societal acceptance especially when exploitation sites are close to protected areas. This session presents a set of examples within Iceland that students and accompanying staff visited in June 2022.

6.1 Þjórsárdalur

According to the National Energy Authority (Orkustofnun), Hydropower accounts for more than 75.5 % of electricity produced in Iceland at 2106 MW of installed capacity. Of this 2106 MW almost half, 1035 MW, of capacity is in the Þjórsá river . Þjórsá (the river of bulls) is Icelandic longest and second most voluminous river: about 230 km long with average discharge 380 m^3/s, originating from Höfsjökull. Due to its glacier origin, Þjórsá divides into a great number of interlinked tributaries. The two largest tributaries are Tungnaá and Kaldakvisl, both originating in Vatnajökull.

As the river continues from the Highlands to Lowlands, diverse topography allows the river to form many waterfalls, amongst all for example Háifoss, Budafoss, Urridafoss or Hestfoss, and little eyots, the largest being Hagaey and Arnes.

Þjórsá and Tungnaa host 6 hydropowerplants with combined capacity of 1035 MW: Búdarhalsvirkjun, Burfellsvirkjun, Sultartangavirkjun, Hrauneyjafossvirkjun, Sigölduvirkjun, Vatnsfellsvirkjun. All of them owned and operated by Landsvirkjun.

This area is of particular interest due to the proximity of the industrialized power sector along the river and the nearby protected areas in both Þjórsárdalur & nearby highland regions of Fjallabak og fríðland and þjórsárver The proximity to the Þjórsárdalur area can be seen in Figure 65: Outline of Protected Area in Þjórsárdalur with proximity of Þjórsá power stations. The protected area is outlined in yellow with the area developed for power production seen outlined in red.

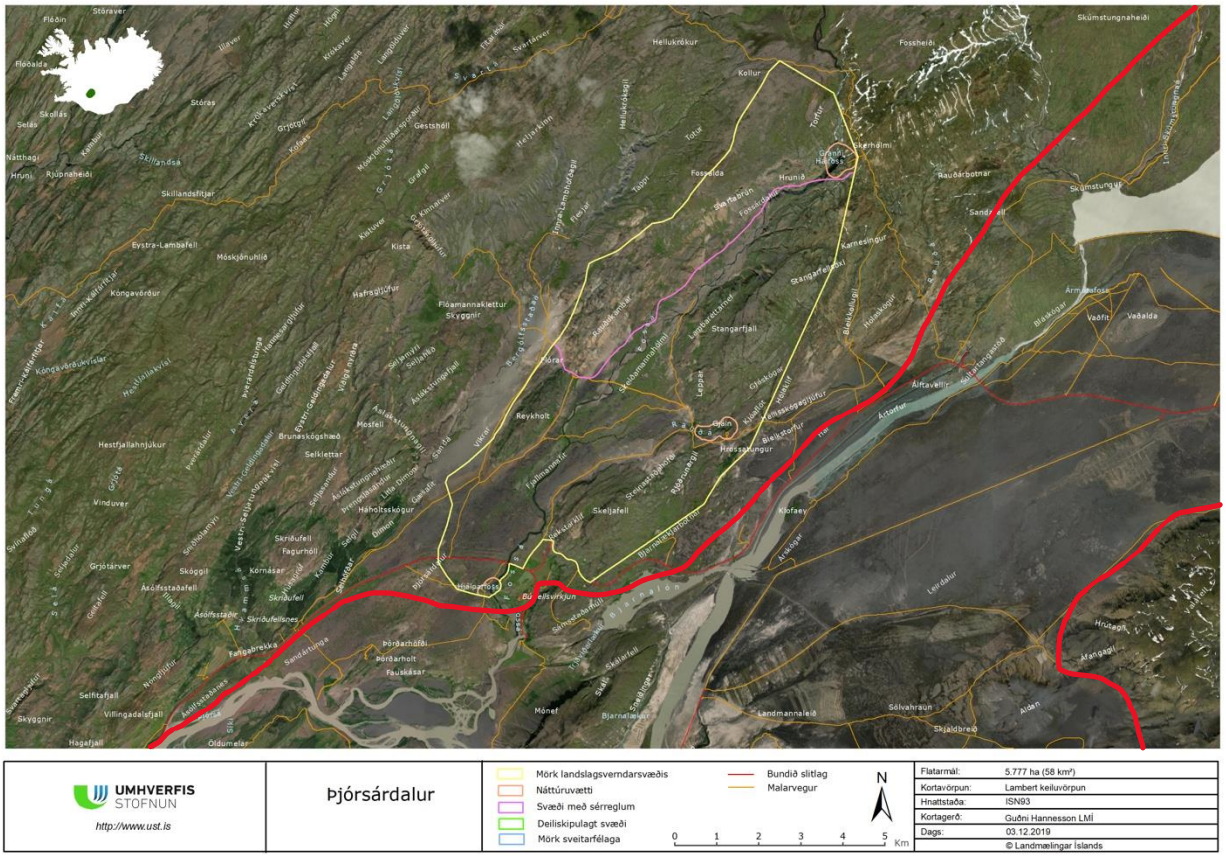

Figure 65: Outline of Protected Area in Þjórsárdalur with proximity of Þjórsá power stations

A map of another protected area in near the Þjórsá area can be seen below in Figure 66: Þjórsárver Protected Areas in a 3D map produced by the Ministry of the Environment – Iceland. A portion of the reservoir systems for the hydro stations along the Þjórsá river seen just beside the yellow dotted line outining the protected area.

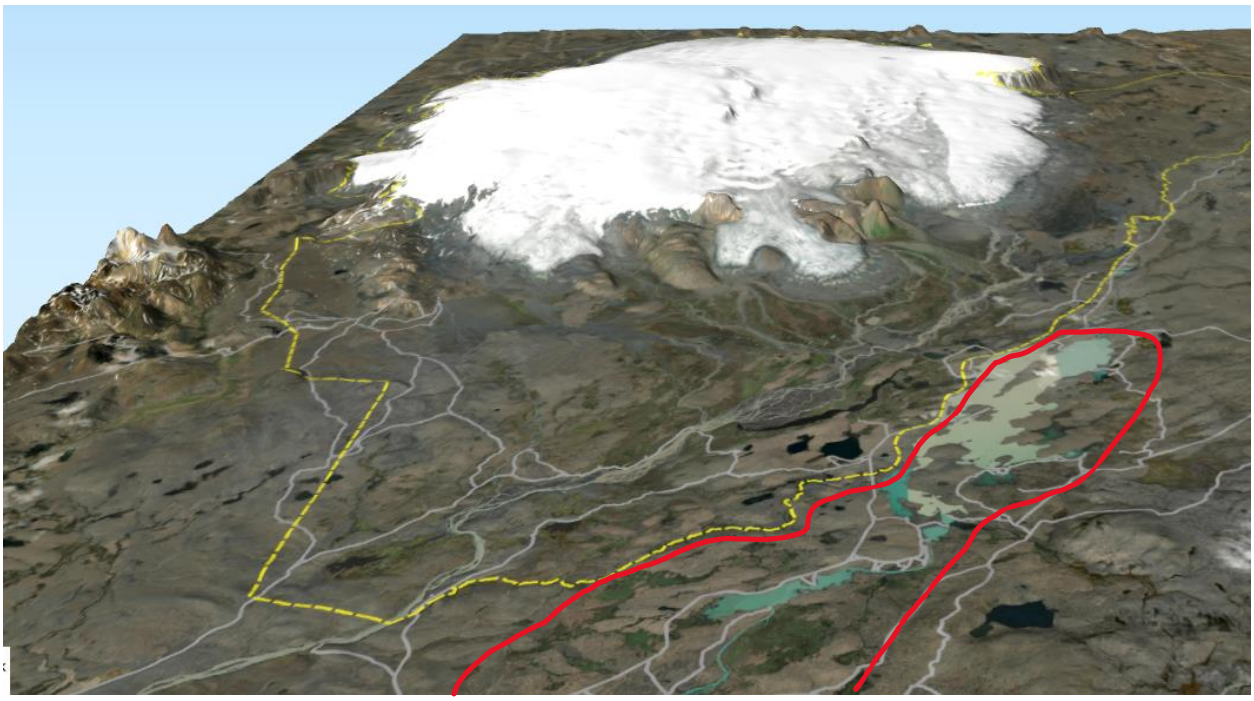

Figure 66: Þjórsárver Protected Areas

It is particularly important for the students to understand the interconnectivity of these areas and how regulators seek to balance interest for industrial development with environmental protection. Visits to this area and associated discussions can help promote an understanding of both the need and interconnectivity of project developments. A key point can be made from discussing Figure 66: Þjórsárver Protected Areas . Despite a certain area being protected, effects from developments downstream can drive changes in the natural environment in the protected areas.

6.2 **Burfellstöð & Gjáin**

Burfell hydro power station in the Þjórsárdalur area, is second biggest power plant after Karahnjúkar hydropower station (690 MW), with installed capacity 370 MW. The power station is located close to Stöng, the Saga-age farm and historic protected site on the river þjórsá. Additionally within the protected area of Þjórsárdalur seen in Figure 65 is the protected area of Gjáin. The visit during the Iceland ISP can be seen below in Figure 67: Geo3en ISP students at Gjáin.

Figure 67: Geo3en ISP students at Gjáin

Nearby Búrfell, and visible from Gjáin, is the site of Hafið where two wind turbines were commissioned in 2013. These two turbines produce 6.7 GW/h a year and were installed as pilot turbines to investigate the feasibility of a 200 MW installation (Mannvit Engineering Consultants). This project however was not included in Iceland´s energy master plan (rammaáætlun) primarily due to its perceived impact on the visual landscape and notably its visibility from Gjáin and Stöng.

While there are no geothermal power plants located in the area, the pitfalls of development are easily presentable during a visit to this area. Stakeholders including project developers must consider a variety of interests when developing a power project including the environment and political issues related to the environment. As Geo3En seeks to produce geothermal engineering graduates with a comprehensive knowledge of the development process, we felt it necessary to show them on-site the potential issues that may arise from the process and promote a discussion about what mitigation techniques can be employed to meet an optimal socio-economic and environmental outcome.

7 Summary

The present deliverable summarizes a series of efforts by the Geo3EN consortium in order for the course catalog presented in IO3 to find applications and case studies in as many disciplines as possible.

It is believed that the visits of powerplants, geological objects, component manufacturers and research laboratories are mandatory activities in order for engineers to be prepared in

1) designing exploration and exploitation strategies to maximize reservoir production,
2) setting up highly efficient surface installations in terms of energy production, transformation and transport,
3) establishing competitive business plans and maximize returns on investments and profits.

This seeking for competitiveness aims at increasing the geothermal energy utilization but it must also take into account the balance between the necessity to fulfill societies increasing energy demands and environmental protection.

The consortium aims at giving the future generation of engineers all the knowledge related tools and experience in order to fulfill the challenge of producing low carbon, clean and secure geothermal energy, at a competitive cost while respecting the environment.